System equivalent model mixing

Klaassen, Steven W.B.; van der Seijs, Maarten V.; de Klerk, Dennis

DOI
10.1016/j.ymssp.2017.12.003

Publication date
2017

Document Version
Accepted author manuscript

Published in
Mechanical Systems and Signal Processing

https://doi.org/10.1016/j.ymssp.2017.12.003

System Equivalent Model Mixing

Steven W.B. Klaassen[a,b], Maarten V. van der Seijs[a,c], Dennis de Klerk[a,c]

[a]*Delft University of Technology, Faculty of Mechanical, Maritime and Material Engineering, Department of Precision and Microsystems Engineering, Section Engineering Dynamics, Mekelweg 2, 2628CD, Delft, The Netherlands*

[b]*Technische Universität München, Faculty of Mechanical Engineering, Institute of Applied Mechanics, Boltzmannstr. 15, 85748 Garching, Germany*

[c]*VIBES.technology, Molengraaffsingel 14, 2629JD Delft, The Netherlands*

Abstract

This paper introduces SEMM: a method based on Frequency Based Substructuring (FBS) techniques that enables the construction of hybrid dynamic models. With System Equivalent Model Mixing (SEMM) frequency based models, either of numerical or experimental nature, can be mixed to form a hybrid model. This model follows the dynamic behaviour of a predefined weighted *master* model. A large variety of applications can be thought of, such as the DoF-space expansion of relatively small experimental models using numerical models, or the blending of different models in the frequency spectrum. SEMM is outlined, both mathematically and conceptually, based on a notation commonly used in FBS. A critical physical interpretation of the theory is provided next, along with a comparison to similar techniques; namely DoF expansion techniques. SEMM's concept is further illustrated by means of a numerical example. It will become apparent that the basic method of SEMM has some shortcomings which warrant a few extensions to the method. One of the main applications is tested in a practical case, performed on a validated benchmark structure; it will emphasize the practicality of the method.

Keywords: System Equivalent Model Mixing, hybrid model, dynamic substructuring, frequency based substructuring, model expansion, trust function

Nomenclature

DoF	degree of freedom
FRF	frequency response function
$\mathbf{u}$	dynamic displacements / rotations
$\mathbf{f}$	applied forces / moments
$\mathbf{g}$	interface forces / moments
$\mathbf{Y}$	admittance FRF matrix
$\mathbf{Z}$	impedance FRF matrix
$\mathbf{T}$	transformation matrix
$\mathbf{B}$	signed Boolean coupling matrix
$\mathbf{C}$	compatibility coupling matrix
$\mathbf{E}$	equilibrium coupling matrix
$\mathbf{L}$	localisation matrix

$\star^{\text{par}}$	pertaining to the parent model
$\star^{\text{ov}}$	pertaining to the overlay model
$\star^{\text{rem}}$	pertaining to the removed model
$\star^{\text{SEMM}}$	pertaining to the SEMM hybrid model
$\star^{+}$	pseudo inverse
$\star_b$	boundary or interface DoF
$\star_i$	internal DoF
$\star_d$	discarded internal DoF
$\star_k$	kept internal DoF
$(+)$	Model coupling
$(-)$	Model decoupling

Email addresses: s.w.b.klaassen@outlook.com (Steven W.B. Klaassen), mvanderseijs@vibestechnology.com (Maarten V. van der Seijs), d.deklerk@tudelft.nl (Dennis de Klerk)

1. Introduction

Structural dynamic analysis is an essential step in the design of high-tech mechanical systems. Complex products such as cars, airplanes, and high-tech machines are designed in an increasingly modular fashion, combining off-the-shelf components with newly designed parts. This generally requires the construction of dynamic models for each component in the system, which can be assembled or 'substructured' together in order to evaluate dynamic properties of the full product, such as global vibration modes or mechanical/acoustical transfer functions. Developments in Dynamic Substructuring (DS) [1–4] have increased the flexibility to combine component models from multiple modelling domains, such that experimentally obtained models may be incorporated with similar ease to numerical models. Still, the component models must fulfil two main requirements: they must correctly depict the dynamic properties of the actual component (e.g. resonance frequencies and damping) and possess clearly defined interfaces for assembling to their adjacent components.

Numerical modelling has long been the industry practice and is particularly strong in the latter: creating models with high spatial resolution from which interface degrees of freedom (DoF) are easily and unambiguously obtained. To correctly represent the dynamics of the actual component, models are often updated with experimental dynamic properties obtained from measurements. Advancement in experimental techniques now also facilitate experimental modelling as an integral means to obtain dynamic models, for instance represented by frequency response functions (FRF) for all relevant interface DoF. This has led to an increase in experimental modelling of relatively complex structures, due to the fact that experimental models offer the dynamic transfers of the mechanical system 'as is', whereas the numerical model offers a 'best-approximated' description.

1.1. Difficulties & remedies in experimental modelling

Yet, standalone experimental models lack the strong suits of the numerical model. It remains challenging to extract a consistent dynamic model from essentially independent (and often imperfect) measurements, performed on a limited number of non-collocated DoF. Many strategies have been proposed to mitigate these shortcomings:

- *Modal fitting*: these techniques fit the observed dynamics (FRF) to an analytical dynamic manifold, expressed by a finite set of (linear) vibration modes with, per definition, consistent dynamic behaviour. However, these methods do not incorporate the full extent of the experimental results; this is mainly because they project all measured physical effects on a model with limited dynamic leeway [5, 6].
- *Expansion using numerical models*: several techniques employ FE-models in order to 'fill in the blanks' between the measured nodes of the experimental FRFs. Static expansion methods like Guyan expansion use the stiffness matrix, sometimes expanded with accelerance terms as is the case with the Improved Reduction System (IRS). Other methods like Hurty Craig-Bampton, SEREP and VIKING also incorporate dynamic behaviour [7–9].
- *Expansion using local rigidness*: a typical shortcoming of experiments is a lack of rotational DoF and inability to express translational/rotational responses at the exact location where forces/moments act (sometimes called *collocated* or *vectorially-associated DoF*). The Virtual Point Transformation solves this by combining multiple translational DoF and assuming that the structure surrounding the interface exhibits rigid behaviour. In essence, this involves an expansion using six rigid Interface Displacement Modes (IDMs) per coupling point, or more if flexible interface behaviour is to be included [10–12].
- *Simulating realistic boundary conditions*: instead of trying to capture the interface dynamics in free conditions, one might also mass-load the interfaces of interest, to be closer to the assembled condition. Substructure coupling and decoupling techniques can be used to remove or replace the surrogate parts. This concept is probably best known as the Transmission Simulator method for use in the modal domain, but can be equally effective in frequency-domain substructuring [13–16].

1.2. Hybrid modelling using SEMM

In the end, the choice between numerical or experimental modelling is made per component based on how the strengths and weaknesses of the respective modelling type best coincide with the requirements of the model. As such, this choice is in fact a compromise. It stands to reason therefore, that the ability to incorporate the strong suits of different modelling techniques into a single model is beneficial. A hybrid model could implement the 'as is' description of the experimental model, combined with the extensive DoF-space and consistency associated with the numerical model.

System Equivalent Model Mixing (SEMM) is a method that means to facilitate the construction of hybrid models based on substructure coupling and decoupling. It applies boundary conditions to a predefined *slave* model such that it behaves as a certain input *master* model. Unlike the methods described above, it does not follow an updating scheme and it does not remove physically relevant information. Furthermore, the SEMM framework is a frequency-independent process; this essentially means that the method choices can be made per frequency line, enhancing mixing flexibility.

1.3. Paper outline

This paper introduces SEMM: a method to mix multiple equivalent models of the same component into one hybrid model. The method is largely based on the Lagrange multiplier frequency-based substructuring (LM-FBS) method [17], hence section 2 commences with a brief revision of this method which will benefit the understanding of SEMM. Next, SEMM is presented mathematically in section 2.2 and then conceptually in section 2.3. Here a critical physical interpretation is given and elaborated with an example in section 2.4. The critical examination will highlight some problems including the presence of spurious peaks.

To remedy these complications, several extensions to the method are examined in section 3. These extensions include the use of an extended interface description in section 3.1, an introduction to unique internal DoF in the master models in section 3.2, and finally the theory on hybrid dynamics is touched upon in section 3.3.

Once the theory is fully expounded, the method is put to practice on a benchmark structure in section 4. In this test case, one of the envisioned practical applications of SEMM will be investigated, namely using SEMM-expanded internal DoF in the construction of high-quality modular system models. A practical investigation into how numerical models can be used to enhance low-frequency content of experimental models is also performed.

2. Theory

This section introduces the basic theory of the SEMM method, starting with a recap of Lagrange multiplier frequency-based substructuring (LM-FBS) which provides the basic framework and notation for the theoretical derivation [2]. As more theory on SEMM is presented, the overlap with FBS methods will become apparent. Indeed, the method is borne by the idea of dynamic substructuring; however, applied to assemble equivalent models of a single component rather than to assemble distinct components.

2.1. Short revision of the LM-FBS method

Let us consider two given structures: components A and B. These components can be coupled dynamically on a predefined interface. The uncoupled equation of motion is presented below. Note that the explicit dependency on frequency is omitted for clarity reasons, as will be done for the remainder of the paper.

$$\mathbf{Zu} = \mathbf{f} + \mathbf{g}, \quad \mathbf{Z} \triangleq \begin{bmatrix} \mathbf{Z}^A & \mathbf{0} \\ \mathbf{0} & \mathbf{Z}^B \end{bmatrix} \tag{1}$$

Here $\mathbf{Z}$ represents the substructures' dynamic stiffness or impedance matrices in block-diagonal form, $\mathbf{f}$ the vector of applied forces to the system and $\mathbf{g}$ the vector of interface forces needed for substructure coupling. When coupled, the system is said to be subject to two sets of constraints or conditions: these are the compatibility and equilibrium condition, represented in matrix notation by (2) and (3) respectively. A signed Boolean matrix $\mathbf{B}$, comprising ones and minus ones on the interface DoF, accounts for the two sets of conditions in an efficient manner:

$$\mathbf{Bu} = \mathbf{0} \tag{2}$$

$$\mathbf{g} = -\mathbf{B}^T\boldsymbol{\lambda} \tag{3}$$

The matrix notation allows for the direct application of these conditions into (1), which in turn can be recast in matrix notation as:

$$\begin{bmatrix} \mathbf{Z} & \mathbf{B}^T \\ \mathbf{B} & \mathbf{0} \end{bmatrix} \begin{bmatrix} \mathbf{u} \\ \boldsymbol{\lambda} \end{bmatrix} = \begin{bmatrix} \mathbf{f} \\ \mathbf{0} \end{bmatrix} \tag{4}$$

The presented system of equations is solved for the coupled displacements $\mathbf{u}$. This results in the single-line method (7), obtained following the derivation below:

$$\begin{aligned} \mathbf{u} &= \mathbf{Z}^{-1}\left(\mathbf{f} - \mathbf{B}^T\boldsymbol{\lambda}\right) \\ \mathbf{Bu} &= \mathbf{BZ}^{-1}\left(\mathbf{f} - \mathbf{B}^T\boldsymbol{\lambda}\right) \qquad\qquad = \mathbf{0} \\ \boldsymbol{\lambda} &= \left(\mathbf{BZ}^{-1}\mathbf{B}\right)^{-1}\mathbf{BZ}^{-1}\mathbf{f} \\ \mathbf{u} &= \left[\mathbf{Y} - \mathbf{YB}^T\left(\mathbf{BYB}^T\right)^{-1}\mathbf{BY}\right]\mathbf{f} \end{aligned} \tag{5}$$

Where $\mathbf{Y}$ represents the uncoupled system admittance model defined as:

$$\mathbf{Y} \triangleq \begin{bmatrix} \mathbf{Y}^A & \mathbf{0} \\ \mathbf{0} & \mathbf{Y}^B \end{bmatrix} = \begin{bmatrix} (\mathbf{Z}^A)^{-1} & \mathbf{0} \\ \mathbf{0} & (\mathbf{Z}^B)^{-1} \end{bmatrix} = \begin{bmatrix} \mathbf{Z}^A & \mathbf{0} \\ \mathbf{0} & \mathbf{Z}^B \end{bmatrix}^{-1} \tag{6}$$

Noting that the terms between the brackets in equation (5) is the transfer from a force $\mathbf{f}$ to the coupled displacements $\mathbf{u}$, the coupled admittance $\bar{\mathbf{Y}}$ is derived as:

$$\bar{\mathbf{Y}} = \mathbf{Y} - \mathbf{YB}^T\left(\mathbf{BYB}^T\right)^{-1}\mathbf{BY} \tag{7}$$

$\bar{\mathbf{Y}}$ is the dually-assembled system model as a result of the LM-FBS procedure, which provides the basis for SEMM coupling and decoupling. Therefore, method (7) will be used throughout the following sections to solve the system equations of SEMM.

2.2. Basic concept of SEMM

2.2.1. The different input models

As the name implies, System Equivalent Model Mixing (SEMM) is a process of mixing equivalent models of a component, yet from different modelling natures. For the following explanation, a naming convention will be used to indicate the different models: the hybrid, parent, overlay and removed model. Each is briefly introduced here, followed by a more in-depth mathematical explanation in the remainder of the section.

1. *Hybrid Model:* the resulting model constructed with SEMM. This model is the result of a SEMM coupling between the input parent and overlay models.
2. *Parent Model:* the model from which the hybrid model inherits the DoF structure, i.e. the hybrid model consists of the same DoF-set as the parent model. However, the parent model will not provide the dynamics to the hybrid model.

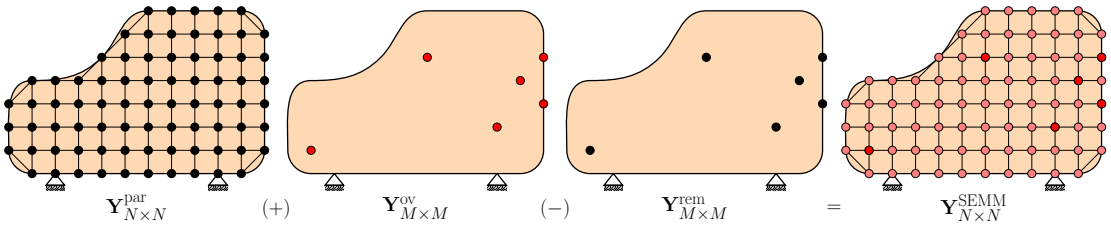

Figure 1: A *parent* model with a large number (N) of DoF (left) is coupled to an *overlay* model with a subset ($M \ll N$) of DoF (centre-left). From this coupled model a subset of the parent model called the *removed model* (centre-right) is decoupled to create a new 'hybrid' formulation (right). This hybrid model has the size (N) of the *parent* model, yet extended with the dynamic information provided by the *overlay* model.

3. *Overlay Model:* the model which provides the dynamic properties by enforcing them onto the parent model. This model's DoF-set is a subset of the parent model's DoF-set.
4. *Removed Model:* this model is a condensed sub-model of the parent model and consists of a subset of DoF of the parent model. The objective of this condensed model is to remove the parent dynamics from the component, in order for it to be replaced by the dynamics of the overlay model.

SEMM is based on the coupling on all shared DoF of two equivalent component models: a *parent* model $\mathbf{Y}^{\text{par}}$ and an *overlay* model $\mathbf{Y}^{\text{ov}}$, defined as follows:

$$\mathbf{Y}^{\text{par}} \triangleq \begin{bmatrix} \mathbf{Y}_{ii} & \mathbf{Y}_{ib} \\ \mathbf{Y}_{bi} & \mathbf{Y}_{bb} \end{bmatrix}^{\text{par}} ; \qquad \mathbf{Y}^{\text{ov}} \triangleq \left[\mathbf{Y}_{bb}\right]^{\text{ov}} \tag{8}$$

The parent DoF are grouped in internal i and boundary DoF b. The internal DoF are unique to the parent model whereas the boundary DoF are shared with the overlay model. Relation (9) states that the overlay model's DoF-set is a subset of the parent model DoF-set[1]. Consequently, all overlay DoF are shared with the parent model[2] and because coupling occurs between all shared DoF the overlay model contains only boundary DoF.

$$\{\mathbf{u}^{\text{ov}}\} \in \{\mathbf{u}^{\text{par}}\} \tag{9}$$

The basis of SEMM is that the overlay model will provide the dynamics to the hybrid model, whereas the parent model provides the DoF-structure. The resulting hybrid model will thereby consist of the entire parent DoF-set $\{\mathbf{u}^{\text{par}}\}$. In fact, the hybrid model can be regarded as a coupled parent model. Figure 1 illustrates how the various models relate.

In order to force the overlay dynamics in the parent model DoF-structure, the original parent model dynamics must first be removed. This is done by decoupling a condensed form of the parent model, namely condensed on the boundary DoF. This model is called the *removed model* $\mathbf{Y}^{\text{rem}}$, defined below:

$$\mathbf{Y}^{\text{rem}} \triangleq \left[\mathbf{Y}_{bb}\right]^{\text{par}} = \left[\mathbf{Z}^{\text{par}}_{bb} - \mathbf{Z}^{\text{par}}_{bi}\left(\mathbf{Z}^{\text{par}}_{ii}\right)^{-1}\mathbf{Z}^{\text{par}}_{ib}\right]^{-1} \tag{10}$$

It should be noted that the removed model is expressed in the admittance notation, therefore it is automatically defined as the condensed form of the parent model. The dynamic stiffness expression on the right-hand side of (10) assumes the form of a Schur complement used in *Guyan reduction*.

[1] The name 'overlay model' derives from this property: the overlay model can be placed over the intersection of the DoF-sets of two given models.

[2] The general application of SEMM does indeed allow for the mixing of two models, each with unique internal DoF; this is done with the introduction of secondary parent models in section 3.2

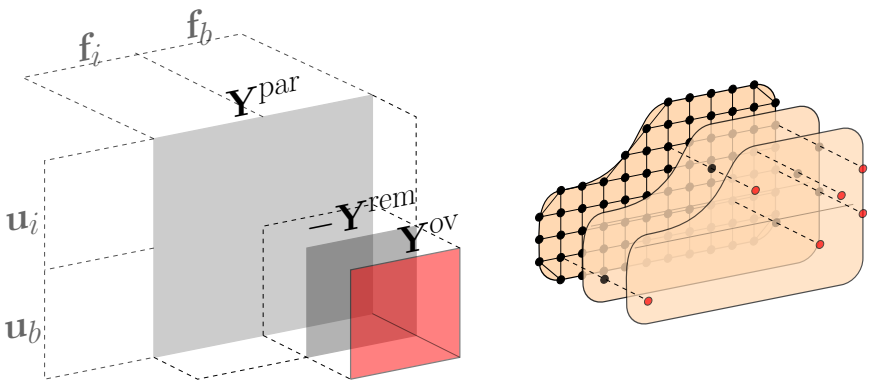

Figure 2: The intersection of the three models is displayed graphically. The *overlay* model $\mathbf{Y}^{\text{ov}}$ is coupled to the *removed interface* model $\mathbf{Y}^{\text{rem}}$. This model is in turn coupled to its parent model $\mathbf{Y}^{\text{par}}$. These relations are described by the signed boolean coupling matrix $\mathbf{B}$. The *overlay* model's name is derived from the fact that it is placed over the other models.

2.2.2. Creating the hybrid model

In order to touch on the physical concept of SEMM, the mathematical theory must first be presented. Once the basic theory is discussed the physical interpretation can be provided. This basic method will be further illustrated with a short example.

Let us start by assuming a system of equations consisting of the three introduced models. Again, applied forces $\mathbf{f}$ and boundary forces $\mathbf{g}$ act on the system. Note that the dynamic stiffness of the removed model is supplied with a minus sign to realise decoupling behaviour.

$$\begin{bmatrix} \mathbf{Z}^{\text{par}} & \mathbf{0} & \mathbf{0} \\ \mathbf{0} & -\mathbf{Z}^{\text{rem}} & \mathbf{0} \\ \mathbf{0} & \mathbf{0} & \mathbf{Z}^{\text{ov}} \end{bmatrix} \begin{bmatrix} \mathbf{u}^{\text{par}} \\ \mathbf{u}^{\text{rem}} \\ \mathbf{u}^{\text{ov}} \end{bmatrix} = \begin{bmatrix} \mathbf{f}^{\text{par}} \\ \mathbf{0} \\ \mathbf{0} \end{bmatrix} - \begin{bmatrix} \mathbf{g}^{\text{par}} \\ \mathbf{g}^{\text{rem}} \\ \mathbf{g}^{\text{ov}} \end{bmatrix} \tag{11}$$

The applied forces act only on the parent model. This is because, as previously stated, the effects on the parent model are of interest; the overlay and removed model are used only to define new boundary conditions on said parent model. These boundary conditions are, as with LM-FBS, the compatibility and equilibrium conditions inherent to DS.

The compatibility relations between the three models read:

$$\mathbf{u}_b^{\text{par}} = \mathbf{u}^{\text{rem}} = \mathbf{u}^{\text{ov}} \quad \Longrightarrow \quad \begin{cases} \mathbf{u}_b^{\text{par}} - \mathbf{u}^{\text{rem}} = \mathbf{0} & \text{(12a)} \\ \mathbf{u}^{\text{rem}} - \mathbf{u}^{\text{ov}} = \mathbf{0} & \text{(12b)} \end{cases}$$

It should be noted that the relation is explicitly made between the parent and removed model, and between the removed and overlay model. By extension, an implicit relation between the parent and the overlay model exists. This relation is displayed graphically in Figure 2.

Next, the equilibrium relation is defined as:

$$\mathbf{g}_b^{\text{par}} + \mathbf{g}^{\text{rem}} + \mathbf{g}^{\text{ov}} = \mathbf{0} \tag{13}$$

Again, these relations can be expressed mathematically in the standard form of (2) and (3) respectively; these are repeated below:

$$\mathbf{B}\mathbf{u} = \mathbf{0} \tag{14}$$

$$\mathbf{g} = -\mathbf{B}^T\boldsymbol{\lambda} \tag{15}$$

This is done by defining a Boolean matrix $\mathbf{B}$ as:

$$\mathbf{B} \triangleq \begin{bmatrix}\mathbf{B}^{\text{par}} & \mathbf{B}^{\text{rem}} & \mathbf{B}^{\text{ov}}\end{bmatrix} = \left[\begin{array}{cc|c|c} \mathbf{0} & -\mathbf{I} & \mathbf{I} & \mathbf{0} \\ \mathbf{0} & \mathbf{0} & -\mathbf{I} & \mathbf{I} \end{array}\right] \tag{16}$$

By implementing the constraints (14) and (15) into the equation of motion (11), the dual dynamic stiffness form is obtained[3]:

$$\begin{bmatrix} \mathbf{Z}^{\text{par}} & \mathbf{0} & \mathbf{0} & \mathbf{B}^{\text{par}T} \\ \mathbf{0} & -\mathbf{Z}^{\text{rem}} & \mathbf{0} & \mathbf{B}^{\text{rem}T} \\ \mathbf{0} & \mathbf{0} & \mathbf{Z}^{\text{ov}} & \mathbf{B}^{\text{ov}T} \\ \mathbf{B}^{\text{par}} & \mathbf{B}^{\text{rem}} & \mathbf{B}^{\text{ov}} & \mathbf{0} \end{bmatrix} \begin{bmatrix} \mathbf{u}^{\text{par}} \\ \mathbf{u}^{\text{rem}} \\ \mathbf{u}^{\text{ov}} \\ \boldsymbol{\lambda} \end{bmatrix} = \begin{bmatrix} \mathbf{f}^{\text{par}} \\ \mathbf{0} \\ \mathbf{0} \\ \mathbf{0} \end{bmatrix} \tag{17}$$

Note that it is now written in the same notation as (4). It can therefore be solved for $\mathbf{u}$ following the single-line method of LM-FBS (7):

$$\bar{\mathbf{Y}} = \mathbf{Y} - \mathbf{Y}\mathbf{B}^T \left(\mathbf{B}\mathbf{Y}\mathbf{B}^T\right)^{-1} \mathbf{B}\mathbf{Y} \quad \text{where} \quad \mathbf{Y} \triangleq \begin{bmatrix} \mathbf{Y}^{\text{par}} & \mathbf{0} & \mathbf{0} \\ \mathbf{0} & -\mathbf{Y}^{\text{rem}} & \mathbf{0} \\ \mathbf{0} & \mathbf{0} & \mathbf{Y}^{\text{ov}} \end{bmatrix} \tag{18}$$

Since SEMM is based on FBS, the same assumptions regarding linearity, time-invariance, and damping that govern FBS models also govern the models in the SEMM process.

2.2.3. Retaining the primal DoF

The coupled model $\bar{\mathbf{Y}}$ is the dually assembled form of the hybrid model. This form has redundant DoF, namely the boundary DoF that appear three times in the system. To retain the unique DoF, use can be made of the localisation matrix $\mathbf{L}$, which is known to be the null space of $\mathbf{B}$ [2]. Although one may select the unique DoF manually, the following is a mathematically correct way [12]:

$$\mathbf{Y}^{\text{SEMM}} = \mathbf{L}^{+} \bar{\mathbf{Y}} \left(\mathbf{L}^{+}\right)^T \tag{19}$$

A simple form of the localisation matrix and a generalised inverse are given here:

$$\mathbf{L} = \left[\begin{array}{cc} \mathbf{I} & \mathbf{0} \\ \mathbf{0} & \mathbf{I} \\ \hline \mathbf{0} & \mathbf{I} \\ \hline \mathbf{0} & \mathbf{I} \end{array}\right] \qquad \Longrightarrow \qquad \mathbf{L}^{+} = \left[\begin{array}{cc|c|c} \mathbf{I} & \mathbf{0} & \mathbf{0} & \mathbf{0} \\ \mathbf{0} & \mathbf{I} & \mathbf{0} & \mathbf{0} \end{array}\right] \tag{20}$$

Note that indeed $\mathbf{B}\mathbf{L} = \mathbf{0}$ and $\mathbf{L}^{+}\mathbf{L} = \mathbf{I}$. Furthermore, this choice of generalised inverse corresponds with the preference to focus on the parent DoF-space. Equation (19) can then be expanded[4] to the single-line method of $\mathbf{Y}^{\text{SEMM}}$:

$$\mathbf{Y}^{\text{SEMM}} = \left[\mathbf{Y}\right]^{\text{par}} - \begin{bmatrix} \mathbf{Y}_{ib} \\ \mathbf{Y}_{bb} \end{bmatrix}^{\text{par}} \left(\mathbf{Y}^{\text{rem}}\right)^{-1} \left(\mathbf{Y}^{\text{rem}} - \mathbf{Y}^{\text{ov}}\right) \left(\mathbf{Y}^{\text{rem}}\right)^{-1} \begin{bmatrix} \mathbf{Y}_{bi} & \mathbf{Y}_{bb} \end{bmatrix}^{\text{par}} \tag{21}$$

Equation (21) is the single-line formulation of the basic form of SEMM. From this equation, two important observations are made:

[3] In fact, the form (17) is nothing more than a substitution coupling. This substitution of sub-components is applied in other coupling techniques; e.g. it is commonplace when using the transmission simulator method [13, 16].

[4] The single-line method for the general form of SEMM of (21) is derived using a primal admittance notation in Appendix A.

1. If the overlay model is equal to, or a reduced form of, the parent model, then the overlay and removed model are identical; thus the second term in (21) is nil and the hybrid model equals the parent model. The mixed model between two identical models is, clearly, that same model.
2. The overlay model $\mathbf{Y}^{\text{ov}}$ which determines the dynamics is not inverted in the process. As a consequence, ill-conditioning due to noise does not explode in the inversion, unlike in classic FBS coupling where noise in the interface is problematic due to the over-stiffening effect of the coupling (see for instance [18]).

2.3. Physical interpretation

The mathematics are interpreted physically as follows: The parent model consists of DoF with a certain spatial relation, defined by the FRF in $\mathbf{Y}^{\text{par}}$. For some of these DoF, i.e. the boundary DoF b, another spatial relation is known: those of the overlay FRF $\mathbf{Y}^{\text{ov}}$. By coupling both models and subsequently decoupling the removed model $\mathbf{Y}^{\text{rem}}$ given by (10), new compatibility and equilibrium conditions are placed on the boundary DoF of the parent model such that these DoF *strictly follow the dynamics of the overlay model*. The behaviour of the remaining unique internal DoF i is imposed by the boundary forces $\mathbf{g}$ acting on the system.

In essence, a reduced coupling interface is used to force dynamic behaviour between models. The use of reduced models to describe full system dynamics is no novelty: reduction techniques have been a study since the 1960s [7, 19] and are aimed on forming equivalent reduced models, which in turn could be used for a variety of applications such as model expansion, optimisation, and updating. Table 1 is a collection of some techniques used today.

Table 1: Some expansion techniques found in literature: how they work and under which conditions [7, 11, 19, 20].

Technique	**Expansion**	**Condition**
Guyan Expansion	$\mathbf{u} = \mathbf{T}\mathbf{u}_b = \begin{bmatrix} -\mathbf{K}_{ii}^{-1}\mathbf{K}_{ib} \\ \mathbf{I} \end{bmatrix} \mathbf{u}_b$	Exact for static boundary-boundary and boundary-internal dynamics. No mass contributions taken into account.
IRS	$\ldots + \begin{bmatrix} \mathbf{K}_{ii}^{-1}\left(\mathbf{M}_{ib} - \mathbf{M}_{ii}\mathbf{K}_{ii}^{-1}\mathbf{K}_{ib}\right) \\ \mathbf{0} \end{bmatrix} \mathbf{M}_{bb}^{-1}\mathbf{K}_{bb}\mathbf{u}_b$	Similar to the Guyan expansion but augmented with an inertia term by means of boundary accelerance.
Dynamic Expansion	$\mathbf{u} = \mathbf{T}\mathbf{u}_b = \begin{bmatrix} -\mathbf{Z}_{ii}^{-1}\mathbf{Z}_{ib} \\ \mathbf{I} \end{bmatrix} \mathbf{u}_b$	Exact for boundary-boundary and boundary-internal dynamics throughout the frequency band.
Hurty Craig-Bampton	$\mathbf{u} = \mathbf{T}\mathbf{u}_b + \mathbf{R}\boldsymbol{\eta}_m = \begin{bmatrix} -\mathbf{K}_{ii}^{-1}\mathbf{K}_{ib} & \boldsymbol{\Phi}_{im} \\ \mathbf{I} & \mathbf{0} \end{bmatrix} \begin{bmatrix} \mathbf{u}_b \\ \boldsymbol{\eta}_m \end{bmatrix}$	In addition to Guyan expansion, internal-internal dynamics are described by a (truncated) set of m internal modes. Modal amplitudes $\boldsymbol{\eta}_m$ are required.
SEREP/VIKING	$\mathbf{u} = \mathbf{T}\mathbf{u}_b = \begin{bmatrix} \boldsymbol{\Phi}_{im}\boldsymbol{\Phi}_{mb}^{+} \\ \boldsymbol{\Phi}_{bm}\boldsymbol{\Phi}_{mb}^{+} \end{bmatrix} \mathbf{u}_b$	Exact expansion for the truncated set of m modes. If $m < b$ smoothing is applied to all DoF in $\mathbf{u}$.
Virtual Point Transformation	$\mathbf{u} = \mathbf{R}\mathbf{q} = \left[\boldsymbol{\Phi}_{\text{IDM}}^{\text{Loc.}}\right] \mathbf{q}$	Expansion of DoF from a virtual set of DoF $\mathbf{q}$ by means of local (rigid) interface displacement modes (IDM).

In the SEMM method, the removed interface model $\mathbf{Y}^{\text{rem}}$ is a reduced form of the parent model $\mathbf{Y}^{\text{par}}$. In fact, by its definition (10), the removed model is the dynamically condensed form of the parent model. Analogously, all expansion methods described in Table 1 state that the expanded model is equivalent to the reduced form where the remainder is deemed negligible, which depending on the conditions can be accurate. More generally, the methods state that the expansion is:

$$\begin{aligned} \mathbf{Y}^{\text{par}} &= \mathbf{T}\mathbf{Y}^{\text{rem}}\mathbf{T}^T + \mathbf{Y}^{\text{res}} \\ \mathbf{Y}^{\text{par}} &\approx \mathbf{T}\mathbf{Y}^{\text{rem}}\mathbf{T}^T \end{aligned} \tag{22}$$

Unlike the expansion techniques described, SEMM states that this residual parent admittance $\mathbf{Y}^{\text{res}}$ is not deemed negligible, thus is not removed from the system. This is because it characterises the dynamics that are uncontrollable by the chosen boundary, better expressed as internal-to-internal dynamics. Furthermore, retaining the residual admittance allows the resulting model to be full rank, which greatly benefits the models' applicability. Nevertheless, by definition, this residual admittance is a property of the parent model and thus conflicts with the overlay dynamics. As a consequence, an error exists which scales with the delta between the overlay and removed model:

$$\epsilon^{\text{res}} \propto \Delta\mathbf{Y} \qquad \Delta\mathbf{Y} = \mathbf{Y}^{\text{ov}} - \mathbf{Y}^{\text{rem}} \tag{23}$$

Fortunately, since the coupling is done between equivalent models, the delta and therefore the error can be assumed small.

Let us now examine this residual parent admittance $\mathbf{Y}^{\text{res}}$. It is defined by a set of modes of the parent model that have nodes on all boundary DoF b. These are the modes of the internal parent model, also called the internal or *fixed-interface modes* as used in the Hurty Craig-Bampton reduction (see for instance [21]). For the internal DoF where this residual lives, it is derived as:

$$\mathbf{Y}^{\text{res}}_{ii} = \mathbf{Y}^{\text{par}}_{ii} - \mathbf{Y}^{\text{par}}_{ib} \left(\mathbf{Y}^{\text{par}}_{bb}\right)^{-1} \mathbf{Y}^{\text{par}}_{bi} \tag{24}$$

Physically the residual describes the motion of a system as if the interface were fixed, i.e. it describes the internal system. As these internal modes have eigenfrequencies much higher than the full system modes, it can be reasoned that the resulting error ϵ^{res} only becomes apparent at higher frequencies. Nonetheless, the error causes undesired spurious peaks in the hybrid model at the internal mode frequencies. This effect will be illustrated with a numerical example in section 2.4.

It can thus be concluded that there are shortcomings to the basic method as presented in the previous section. The apparent limitations of the basic method are the following:

1. The existence of conflicting dynamics due to the residual admittance $\mathbf{Y}^{\text{res}}$ causes spurious peaks in the hybrid model at internal mode frequencies. In 3.1 this problem is addressed by redefining the removed model $\mathbf{Y}^{\text{rem}}$.

2. Relation (9) states that the overlay DoF-set is a subset of the parent DoF-set. This evokes a serious limitation to the overlay model's size. Certainly, both input models could generally consist of DoF not present in the other, i.e. both could contain unique internal DoF i. Relation (9) of the basic method decides however, that the overlay model contains only boundary DoF and has no room for internal DoF that might be of interest. This limits the size of the hybrid model. In 3.2 this problem is resolved with the introduction of a secondary parent set.

3. As the dynamics of the hybrid model are defined by the overlay model only, the parent dynamics are dismissed entirely. In fact, the method revolves around the removal of parent and the insertion of overlay dynamics, as illustrated in Figure 1. Nonetheless, there are situations or frequency ranges where the parent model is the more trusted source of dynamics. The basic method does not facilitate parent model dynamics in the hybrid model. This is circumvented in 3.3 by redefining the source of the overlay model, hence permitting to 'fade in' dynamics of the parent into the overlay.

2.4. Numerical example: a truss construct

For this example a simple truss-construct is created with the use of simple bar elements (figure 3). It is modelled in two manners, each with different mechanical properties. The first model is used as the parent. The second model is condensed on a subset of DoF to form the overlay model. Rayleigh damping is used for both models; the Rayleigh damping coefficients α and β are provided along with other mechanical properties in Table 2.

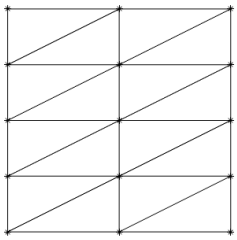

Figure 3: A Numerical truss-frame structure created with bar elements. There are $15 \times 2 = 30$ DoF. The top three nodes are fixed for both the parent and overlay models.

Due to the differences in the properties of the bar elements, the eigenmodes of the parent and overlay model are at a slight off-set from one another. Although the two are equivalent — as they describe the same system — both offer different predictions on the system dynamics. In Table 3 the eigenfrequencies of the parent and overlay model are listed. Additionally the fixed-boundary modes of the parent $\mathbf{Y}^{\text{par}}$ are provided.

Table 2: The mechanical properties of the truss construction for the parent $\mathbf{Y}^{\text{par}}$ and overlay $\mathbf{Y}^{\text{ov}}$ model.

Properties	Parent		Overlay	
Area	64	mm^2	36	mm^2
E-Modulus	110	GPa	120	GPa
Density	7800	kg/m^3	7800	kg/m^3
α	5e-6	[-]	1e-6	[-]
β	1e-8	[-]	1e-8	[-]

Table 3: The eigenfrequencies of the Parent $\mathbf{Y}^{\text{par}}$ and Overlay $\mathbf{Y}^{\text{ov}}$ are provided on the left. On the right the fixed-boundary modes of the parent model are also given. Note that the fixed-boundary modes of the parent model act at much higher frequencies than the free-modes of the parent model, as expected.

Mode	Eigenfrequencies [Hz]		Mode	Eigenfrequencies [Hz]
	Parent $\mathbf{Y}^{\text{par}}$	Overlay $\mathbf{Y}^{\text{ov}}$		Fixed-boundary modes of the parent model
1	137	143	1	866
2	410	428	2	899
3	476	497	3	1120
4	820	856	4	1190
5	930	971	5	1376
6	1169	1221	6	1457
7	1240	1295	7	1809
8	1385	1446	8	2070

Let us apply a dynamic load-case. It is explained in the previous section that the residual $\mathbf{Y}^{\text{res}}$ contains the fixed-boundary eigenmodes of the parent model. Since the hybrid model contains this residual, it is sensitive to the eigenfrequencies of this fixed internal system resulting in spurious peaks. Figure 4 is a plot of a driving-point FRF of an internal DoF in the truss-construct. Note that the hybrid model does indeed have spurious peaks at these fixed-boundary modes.

2.4.1. The low-frequency case

The system is first actuated by a harmonic load at $420\,\text{Hz}$ (Denoted by a dotted line in Figure 4). Note that it is in the regime relatively unaffected by the error caused by the residual.

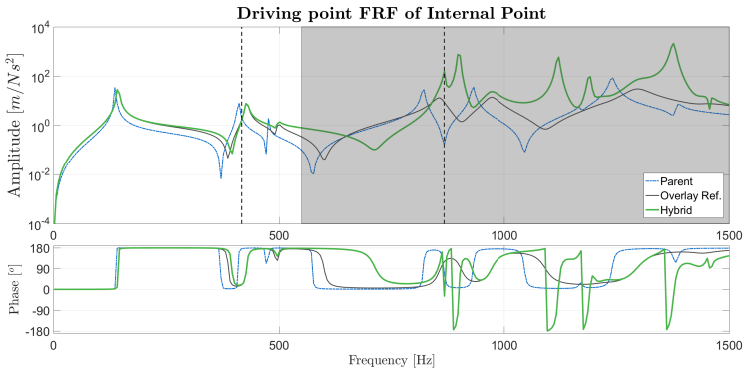

Figure 4: A driving-point FRF of an internal DoF in the truss construct. The hybrid model follows the overlay model for the lower frequencies. At higher frequencies, illustrated by the shaded area, contributions of the fixed-boundary system become more dominant resulting in spurious peaks; the first one appearing at its first eigenfrequency (866 Hz). The vertical dotted lines denote the harmonic load frequencies applied to the system in the following cases.

Figure 5 displays the response of the truss-construct for the different model configurations. The parent model has explicit information on all DoF and shows a vastly different response than the overlay which only has explicit information on a few nodes (illustrated by the black stars). However, by forcing the parent boundary DoF to behave as the overlay boundary DoF the resulting hybrid model provides the explicit response of the implicit overlay model rather accurately. Note that the boundary DoF as configured by both the hybrid and overlay model are in the exact same positions as required by the method.

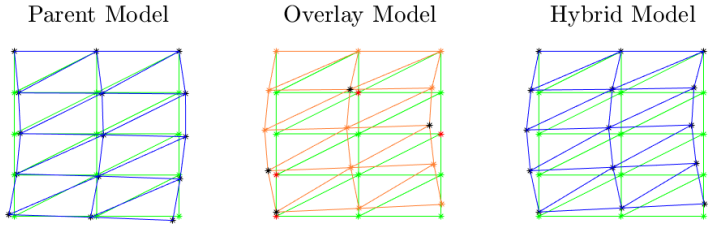

Figure 5: A truss construct actuated by a force at 420 Hz. Both a parent and overlay model exist and both predict different responses to the same load. Furthermore, the parent model (left) describes all nodes whereas the overlay model (centre) describes only a few, marked with a black star. SEMM is applied to create a model with the DoF of the parent model and provides the response of the overlay model.

2.4.2. The high-frequency case

To demonstrate that it is indeed this parent residual that causes the spurious peak, a uniform harmonic load at the first fixed-boundary eigenfrequency (the vertical dotted line in the shaded area of Figure 4 at 866 Hz) is now applied to the system.

The responses of the truss-system, as predicted by the various models, are given in Figure 6. The responses of the system as predicted by both the parent and overlay model are barely observed. However, as seen in the FRF in Figure 4, the hybrid model is sensitive to the first fixed-boundary eigenfrequency; therefore the response is that of the corresponding fixed-boundary eigenmode. This unwanted error is a consequence of a discrepancy caused by the residual parent admittance $\mathbf{Y}^{\text{res}}$ defined by the fixed-boundary system. It becomes apparent that the choice of boundary DoF for the overlay model is of importance. With the standard implementation of SEMM, the boundary DoF-set must be chosen such that the residual system is as stiff as possible, thus decreasing the residual admittance and shifting the fixed-boundary eigenmodes to higher frequencies. This can be interpreted as the DoF-set's ability to properly represent the system's behaviour;

affected by the spatial and modal distribution of the selected boundary DoF.

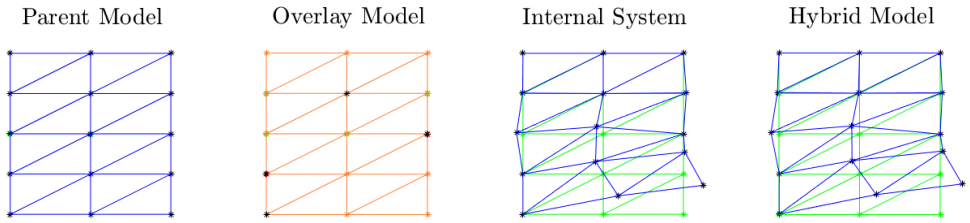

Figure 6: The response of the truss-system under a uniform harmonic load at 866 Hz. Both the parent (left) and overlay model (centre-left) barely respond. In contrast, The internal system of the parent model and therefore the residual $\mathbf{Y}^{\text{res}}$ has its first mode at this frequency (centre-right). Consequently, the hybrid model (right) is sensitive to this actuation.

3. Extensions to the method

The previous chapter introduced the basic method of SEMM, which allows two equivalent models to be combined to form a hybrid model. However, the method is rather restricted, as SEMM is, in fact, a framework for model mixing. In this chapter, three extensions to SEMM are presented. In section 3.1 an extension is introduced which combats the spurious peaks by redefining the removed interface in the decoupling step. In section 3.2 the foundation of the overlay model is broadened. A secondary set of internal DoF – unique to the overlay model – is included as a secondary parent model. Finally in section 3.3 trust functions are introduced, that facilitate the shifting of the dynamic source to either the parent or overlay model.

3.1. The extended interface

In sections 2.3 and 2.4 the concept of the residual parent admittance in the SEMM method is introduced. This residual, although physically relevant, does conflict with the overlay model dynamics: it causes spurious peaks in the dynamic domain of the internal parent system.

Unfortunately, this residual is a direct consequence of unobserved motion and cannot be removed. However, the nature of the residual parent admittance can be controlled. If the residual is defined by the limited observability and controllability of the chosen interface on the parent model, then extending this interface should improve the method. Indeed, including internal DoF in the decoupling of a substructure from a system model has been found to improve on the accuracy of model decoupling; see for instance [14, 15, 22]. The decoupling and thus removal of the parent dynamics can be made cleaner by decoupling an extended definition of the interface. Instead of removing only the boundary DoF, some of the unique internal DoF of the parent set of DoF are included in the decoupling step's compatibility and equilibrium conditions.

The unique internal parent DoF-set denoted by i is decomposed into a set of discarded and kept DoF, respectively denoted by d and k. Note that this decomposition can be done differently for the output and input DoF such that non-square interfaces are created.

$$\mathbf{u}_i = \begin{bmatrix} \mathbf{u}_{d_c} \\ \mathbf{u}_{k_c} \end{bmatrix} \quad \mathbf{f}_i = \begin{bmatrix} \mathbf{f}_{d_e} \\ \mathbf{f}_{k_e} \end{bmatrix} \tag{25}$$

Where the subscripts in the decomposition (d_e, k_e) and (d_c, k_c) stand for equilibrium and compatibility respectively. The removed interface is extended to include the kept unique internal DoF. As a result, the removed interface model is redefined as follows:

$$\mathbf{Y}^{\text{rem}} \triangleq \begin{bmatrix} \mathbf{Y}_{k_c k_e} & \mathbf{Y}_{k_c b} \\ \mathbf{Y}_{b k_e} & \mathbf{Y}_{bb} \end{bmatrix}^{\text{par}} \tag{26}$$

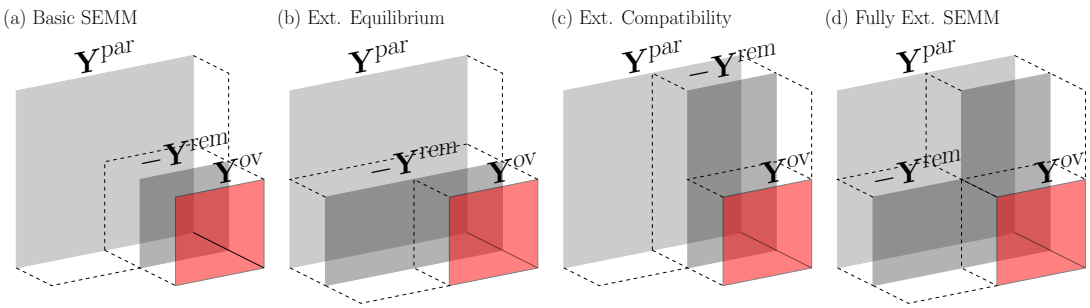

Figure 7: Depending on the choice of kept and discarded DoF the removed interface can be extended to include unique internal DoF in the decoupling step. (a): All internal DoF are discarded ($f_i = f_{d_e}$, $u_i = u_{d_c}$); this is the same as applying the basic method. (b): All the internal input DoF are kept in the equilibrium and all are discarded in the compatibility condition ($f_i = f_{k_e}$, $u_i = u_{d_c}$). (c): Conversely, all the internal input DoF are kept in the compatibility and all are discarded in the equilibrium condition ($f_i = f_{d_e}$, $u_i = u_{k_c}$).(d): All the internal DoF in both the equilibrium and compatibility conditions are kept ($f_i = f_{k_e}$, $u_i = u_{k_c}$). Note that all forms between the minimum of (a) and the maximum of (d) can exist.

It is important to note that the choice of kept and discarded DoF is made separately for the compatibility and equilibrium conditions, allowing the creation of non-square matrices $\mathbf{Y}^{\text{rem}}$. This is clearly depicted in Figure 7 where configuration (b) and (c) show non-square definitions of the removed model. Because of this, the coupling matrix introduced in equation (16) may now be defined separately for the compatibility and equilibrium conditions:

$$\mathbf{C} \triangleq \begin{bmatrix} \mathbf{C}^{\text{par}} & \mathbf{C}^{\text{rem}} & \mathbf{C}^{\text{ov}} \end{bmatrix} = \begin{array}{c} \begin{matrix} d_c & k_c & b & k_c & b & b \end{matrix} \\ \left[\begin{array}{ccc|c|c} \mathbf{0} & -\mathbf{I} & \mathbf{0} & \mathbf{I} & \mathbf{0} & \mathbf{0} \\ \mathbf{0} & \mathbf{0} & -\mathbf{I} & \mathbf{0} & \mathbf{I} & \mathbf{0} \\ \mathbf{0} & \mathbf{0} & \mathbf{0} & \mathbf{0} & -\mathbf{I} & \mathbf{I} \end{array}\right] \end{array} \tag{27a}$$

$$\mathbf{E} \triangleq \begin{bmatrix} \mathbf{E}^{\text{par}} & \mathbf{E}^{\text{rem}} & \mathbf{E}^{\text{ov}} \end{bmatrix} = \begin{array}{c} \begin{matrix} d_e & k_e & b & k_e & b & b \end{matrix} \\ \left[\begin{array}{ccc|c|c} \mathbf{0} & -\mathbf{I} & \mathbf{0} & \mathbf{I} & \mathbf{0} & \mathbf{0} \\ \mathbf{0} & \mathbf{0} & -\mathbf{I} & \mathbf{0} & \mathbf{I} & \mathbf{0} \\ \mathbf{0} & \mathbf{0} & \mathbf{0} & \mathbf{0} & -\mathbf{I} & \mathbf{I} \end{array}\right] \end{array} \tag{27b}$$

Using the coupling matrices of (27a) and (27b), the equation of motion becomes:

$$\begin{bmatrix} \mathbf{Z}^{\text{par}} & \mathbf{0} & \mathbf{0} & \mathbf{E}^{\text{par}T} \\ \mathbf{0} & -\mathbf{Z}^{\text{rem}} & \mathbf{0} & \mathbf{E}^{\text{rem}T} \\ \mathbf{0} & \mathbf{0} & \mathbf{Z}^{\text{ov}} & \mathbf{E}^{\text{ov}T} \\ \mathbf{C}^{\text{par}} & \mathbf{C}^{\text{rem}} & \mathbf{C}^{\text{ov}} & \mathbf{0} \end{bmatrix} \begin{bmatrix} \mathbf{u}^{\text{par}} \\ \mathbf{u}^{\text{rem}} \\ \mathbf{u}^{\text{ov}} \\ \boldsymbol{\lambda} \end{bmatrix} = \begin{bmatrix} \mathbf{f}^{\text{par}} \\ \mathbf{0} \\ \mathbf{0} \\ \mathbf{0} \end{bmatrix} \tag{28}$$

Equation (28) is solved using LM-FBS (7) to obtain the dual hybrid model $\bar{\mathbf{Y}}$. To obtain the primal variant, the following localizing matrices are used:

$$\mathbf{L}_E \triangleq \text{null}\{\mathbf{E}\} \tag{29a}$$

$$\mathbf{L}_C \triangleq \text{null}\{\mathbf{C}\} \tag{29b}$$

Such that the primal model becomes:

$$\mathbf{Y}^{\text{SEMM}} = \mathbf{L}_E^{+}\, \bar{\mathbf{Y}}\, (\mathbf{L}_C^{+})^T \tag{30}$$

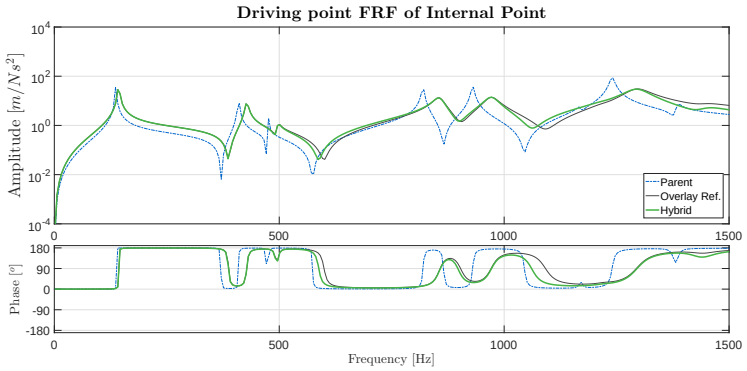

Figure 8: A driving-point FRF of an internal DoF in the truss construct of Figure 5. With the extension of the boundary conditions in the decoupling step of SEMM, the spurious peaks are removed. The hybrid model now follows the reference model throughout the frequency band.

Again, generalized inverses exist for both $\mathbf{L}_E$ and $\mathbf{L}_C$ analogue to the one presented in (20). The associated single-line method is denoted below, which is derived following the primal admittance notation in Appendix A.

$$\mathbf{Y}^{\text{SEMM}} = [\mathbf{Y}]^{\text{par}} - \begin{bmatrix} \mathbf{Y}_{ik_e} & \mathbf{Y}_{ib} \\ \mathbf{Y}_{bk_e} & \mathbf{Y}_{bb} \end{bmatrix}^{\text{par}} \left(\begin{bmatrix} \mathbf{Y}_{bk_e} & \mathbf{Y}_{bb} \end{bmatrix}^{\text{rem}} \right)^{+} (\mathbf{Y}_{bb}^{\text{rem}} - \mathbf{Y}^{\text{ov}}) \left(\begin{bmatrix} \mathbf{Y}_{k_c b} \\ \mathbf{Y}_{bb} \end{bmatrix}^{\text{rem}} \right)^{+} \begin{bmatrix} \mathbf{Y}_{k_c i} & \mathbf{Y}_{k_c b} \\ \mathbf{Y}_{bi} & \mathbf{Y}_{bb} \end{bmatrix}^{\text{par}} \tag{31}$$

By extending the decoupling interface the relationship between the internal system and the boundary system is redefined. Including an internal DoF in the removed model physically accounts to removing the connection between said internal DoF and the boundary system, i.e. the internal-to-boundary and boundary-to-internal dynamics. Consequently, a fully extended interface removes the connection between the boundary and internal system resulting in free behaviour of the internal system. This, in turn, removes the rigid or fixed-boundary behaviour in the residual $\mathbf{Y}^{\text{res}}$, i.e. it removes the spurious peaks at fixed-boundary modes.

It should be noted however, that this in itself introduces another erroneous assumption: The physical connection which is removed in the extended interface configurations does indeed exist, therefore scenario's can be thought of where accepting some if not all physical connections is preferred.

The extended interface for the truss-construct

To demonstrate the effects of the extended interface, the example of the previous section is repeated. This time, a hybrid model is constructed with (31) where all internal DoF are kept following the schematic depicted in Figure 7d. In Figure 8 the same driving-point FRF as before is shown for the new scenario. Unlike the hybrid FRF constructed with the basic method, the FRF constructed with the extended decoupling interface contains no spurious peaks. This is a consequence of the hybrid model no longer being sensitive to the fixed-boundary system.

The performance of the configurations in Figure 7b and Figure 7c are not demonstrated here as the effects of an extended interface are best illustrated by the configuration in Figure 7d. This is because for these configurations, since a physical connection still exists, there is still a sensitivity to the fixed-boundary dynamics albeit in a lesser form.

3.2. The secondary parent model

In the most general form of SEMM, the two combined models can each have unique internal DoF. In other words, two parent models exist: a primary and a secondary parent model, respectively denoted by $\mathbf{Y}^{\text{par,1}}$

and $\mathbf{Y}^{\text{par,2}}$. They are defined as:

$$\mathbf{Y}^{\text{par,1}} \triangleq \begin{bmatrix} \mathbf{Y}_{ii} & \mathbf{Y}_{ib} \\ \mathbf{Y}_{ib} & \mathbf{Y}_{bb} \end{bmatrix}^{\text{par,1}} \quad ; \quad \mathbf{Y}^{\text{par,2}} \triangleq \begin{bmatrix} \mathbf{Y}_{ii} & \mathbf{Y}_{ib} \\ \mathbf{Y}_{ib} & \mathbf{Y}_{bb} \end{bmatrix}^{\text{par,2}}$$

SEMM is now performed in two directions as illustrated in Figure 9. For each parent model a subset is removed; this can be done following either the normal configuration or with the extended interface method. The removed interfaces are defined as:

$$\mathbf{Y}^{\text{rem,1}} \triangleq \begin{bmatrix} \mathbf{Y}_{k_c k_e} & \mathbf{Y}_{k_c b} \\ \mathbf{Y}_{b k_e} & \mathbf{Y}_{bb} \end{bmatrix}^{\text{par,1}} \quad ; \quad \mathbf{Y}^{\text{rem,2}} \triangleq \begin{bmatrix} \mathbf{Y}_{k_c k_e} & \mathbf{Y}_{k_c b} \\ \mathbf{Y}_{b k_e} & \mathbf{Y}_{bb} \end{bmatrix}^{\text{par,2}}$$

The overlay model can be adopted from either parent model[5]. For now, let us state that the overlay model is taken from the secondary parent model, thus staying in line with the theory:

$$\mathbf{Y}^{\text{ov}} \triangleq \left[\mathbf{Y}_{bb}\right]^{\text{par,2}}$$

The coupling matrices are extended with the relations to the secondary model. The compatibility and

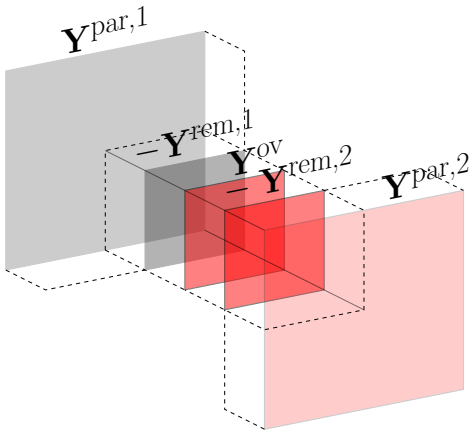

Figure 9: The SEMM concept can be extended with the secondary parent model. The secondary parent model is the model from which the overlay model is extracted. SEMM can be performed in both directions.

equilibrium matrices now read:

$$\mathbf{C} \triangleq \begin{bmatrix} \mathbf{C}^{\text{par,1}} & \mathbf{C}^{\text{par,2}} & \mathbf{C}^{\text{rem,1}} & \mathbf{C}^{\text{rem,2}} & \mathbf{C}^{\text{ov}} \end{bmatrix} \tag{32a}$$

$$\mathbf{E} \triangleq \begin{bmatrix} \mathbf{E}^{\text{par,1}} & \mathbf{E}^{\text{par,2}} & \mathbf{E}^{\text{rem,1}} & \mathbf{E}^{\text{rem,2}} & \mathbf{E}^{\text{ov}} \end{bmatrix} \tag{32b}$$

Again, the combined equations can be recast in matrix form. Note that the applied force vector is extended with secondary parent forces, that actually allow to excite the full DoF-space of both models (which was not the case with the standard definition of the overlay model). Consequently, cross terms now exist between secondary and primary parent models; the models are linked through the overlay model.

$$\begin{bmatrix} \mathbf{Z}^{\text{par,1}} & \mathbf{0} & \mathbf{0} & \mathbf{0} & \mathbf{0} & \mathbf{E}^{\text{par,1}T} \\ \mathbf{0} & \mathbf{Z}^{\text{par,2}} & \mathbf{0} & \mathbf{0} & \mathbf{0} & \mathbf{E}^{\text{par,2}T} \\ \mathbf{0} & \mathbf{0} & -\mathbf{Z}^{\text{rem,1}} & \mathbf{0} & \mathbf{0} & \mathbf{E}^{\text{rem,1}T} \\ \mathbf{0} & \mathbf{0} & \mathbf{0} & -\mathbf{Z}^{\text{rem,2}} & \mathbf{0} & \mathbf{E}^{\text{rem,2}T} \\ \mathbf{0} & \mathbf{0} & \mathbf{0} & \mathbf{0} & \mathbf{Z}^{\text{ov}} & \mathbf{E}^{\text{ov}T} \\ \mathbf{C}^{\text{par,1}} & \mathbf{C}^{\text{par,2}} & \mathbf{C}^{\text{rem,1}} & \mathbf{C}^{\text{rem,2}} & \mathbf{C}^{\text{ov}} & \mathbf{0} \end{bmatrix} \begin{bmatrix} \mathbf{u}^{\text{par,1}} \\ \mathbf{u}^{\text{par,1}} \\ \mathbf{u}^{\text{rem,2}} \\ \mathbf{u}^{\text{rem,2}} \\ \mathbf{u}^{\text{ov}} \\ \boldsymbol{\lambda} \end{bmatrix} = \begin{bmatrix} \mathbf{f}^{\text{par,1}} \\ \mathbf{f}^{\text{par,2}} \\ \mathbf{0} \\ \mathbf{0} \\ \mathbf{0} \\ \mathbf{0} \end{bmatrix} \tag{33}$$

[5] In fact, the overlay model can even adopt a mixed definition of both models; this is the subject of 3.3.

By solving (33), a full system is derived including the internal DoF of both parent models and the interactions therein. These interactions are however 'bottlenecked' through the interface defined by the overlay. Therefore, for these interactions, it is doubly as important that the interface adequately describes the system dynamics.

3.3. Trust function

The overall dynamics of the resulting hybrid model are determined by definition of the overlay. However, as explained in the previous section, the overlay can be extracted from either input parent model. Consequently, the overall dynamics can be steered towards the dynamics defined by either parent model. In fact, this choice can be made per frequency step; the overlay can, for example, be extracted from the model deemed most trustworthy at that particular frequency.

Naturally, the resulting model would contain sharp jumps at frequencies where the overlay's definition is shifted from one parent to the other. Therefore, it would be beneficial if near these shift-frequencies the overlay dynamics can be recast as a weighted mix of both parent models, such that smooth transitions can be made from one to the other parent model. For this to occur, it is required that in these transition zones hybrid dynamics are defined and that these hybrid dynamics can be tuned or faded.

The hybrid dynamics can be created by artificially increasing the influence of either model in a SEMM coupling. The influence of a model in an assembly is determined by the relative stiffness of the models at the boundary. It follows that by weakening the stiffness of the overlay relative to the parent model its influence in the resulting model decreases. This can be achieved by including a symmetric frequency-dependent weighting matrix called the trust function $\mathbf{W}(\omega)$ in the compatibility and equilibrium conditions. The function's name derives from the fact that it tries to quantify the frequency-dependent trust one has in a given model. It is defined as follows:

$$\mathbf{W}(\omega) \in \mathcal{R}^2 : [\mathbf{0}, \mathbf{I}] \;\; \text{Where} \;\; \mathbf{W} = \mathbf{W}^T \tag{34}$$

This function is implemented in the compatibility and equilibrium conditions between the parent and removed model. For example, the compatibility conditions become:

$$\mathbf{W}(\omega)\mathbf{u}_b^{\text{par}} = \mathbf{u}^{\text{rem}} = \mathbf{u}^{\text{ov}} \quad \Longrightarrow \quad \begin{cases} \mathbf{W}(\omega)\mathbf{u}_b^{\text{par}} + \mathbf{u}^{\text{rem}} = \mathbf{0} & \text{(35a)} \\ \mathbf{u}^{\text{rem}} + \mathbf{u}^{\text{ov}} \;\; = \mathbf{0} & \text{(35b)} \end{cases}$$

Essentially, the compatibility now states that for every unit displacement of the removed interface DoF, and by extension overlay DoF, there is $\mathbf{W}(\omega)$ units displacement of the parent DoF. Similarly, the equilibrium conditions are altered; it is stated that the sum of interface forces of the removed and overlay model is equal but opposite to the weighted parent interface forces, which can be denoted as:

$$\mathbf{W}(\omega)\mathbf{g}_b^{\text{par}} = -\left(\mathbf{g}^{\text{rem}} + \mathbf{g}^{\text{ov}}\right) \quad \Longrightarrow \quad \mathbf{W}(\omega)\mathbf{g}_b^{\text{par}} + \mathbf{g}^{\text{rem}} + \mathbf{g}^{\text{ov}} = \mathbf{0} \tag{36}$$

The weighting matrix $\mathbf{W}(\omega)$ is easily implemented in the coupling matrix $\mathbf{B}$:

$$\mathbf{B} \triangleq \begin{bmatrix} \mathbf{W}(\omega)\mathbf{B}^{\text{par}} & \mathbf{B}^{\text{rem}} & \mathbf{B}^{\text{ov}} \end{bmatrix} = \left[\begin{array}{cc|c|c} \mathbf{0} & -\mathbf{W}(\omega) & \mathbf{I} & \mathbf{0} \\ \mathbf{0} & \mathbf{0} & -\mathbf{I} & \mathbf{I} \end{array}\right] \tag{37}$$

By inserting the weighting matrix in the coupling matrix we allow for a gap/discrepancy to exist in both the displacement compatibilities and the force equilibria at the interface. This effectively means that the interface is to some degree compliant; a concept that is more often used in dynamic substructuring to model the effects of joints [23, 24]. In this case however, the interface dynamics are unknown as they are a consequence of the required response, i.e. the required force and displacement gaps. Note that if the weighting matrix is identity, no weakening occurs and normal SEMM is applied. The system equation is

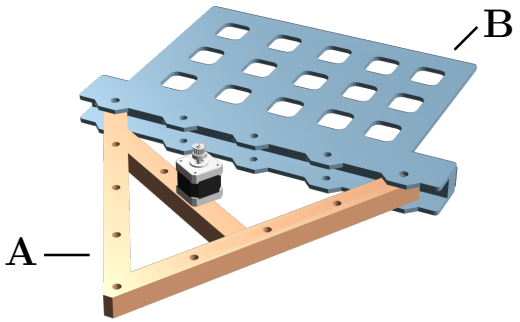

Figure 10: Substructuring benchmark structure [25] used to demonstrate the practical application of SEMM. The structure consists of substructures A and B which are coupled together at two coupling points to form assembly AB.

once again put in the dual admittance form:

$$\begin{bmatrix} \mathbf{Z}^{\text{par}} & \mathbf{0} & \mathbf{0} & \mathbf{B}^{\text{par}T}\mathbf{W}^{T}(\omega) \\ \mathbf{0} & -\mathbf{Z}^{\text{rem}} & \mathbf{0} & \mathbf{B}^{\text{rem}T} \\ \mathbf{0} & \mathbf{0} & \mathbf{Z}^{\text{ov}} & \mathbf{B}^{\text{ov}T} \\ \mathbf{W}(\omega)\mathbf{B}^{\text{par}} & \mathbf{B}^{\text{rem}} & \mathbf{B}^{\text{ov}} & \mathbf{0} \end{bmatrix} \begin{bmatrix} \mathbf{u}^{\text{par}} \\ \mathbf{u}^{\text{par}} \\ \mathbf{u}^{\text{ov}} \\ \boldsymbol{\lambda} \end{bmatrix} = \begin{bmatrix} \mathbf{f}^{\text{par}} \\ \mathbf{0} \\ \mathbf{0} \\ \mathbf{0} \end{bmatrix} \tag{38}$$

The system equation is solved for $\mathbf{u}$ as before using the LM-FBS formulation of equation (7). Theoretically, the resulting tuned model $\mathbf{Y}^{\text{tuned}}$ follows the dynamics as defined by the trust-function. Unfortunately however, the internal DoF $\mathbf{Y}^{\text{tuned}}_{ii}$ are sensitive to the weakening brought about by the trust-function resulting in spurious peak at frequencies where $\mathbf{W}(\omega)$ approaches identity.

Nevertheless, the boundary DoF, which are fully controlled by both overlay and parent models, effectively carry the user-defined hybrid dynamics. Therefore, $\mathbf{Y}^{\text{tuned}}_{bb}$ is a proper overlay model which can be used in any of the SEMM configurations. By definition, the internal DoF will follow the tuned dynamics of $\mathbf{Y}^{\text{tuned}}_{bb}$. As no weakening is performed in these configurations no spurious peak occurs. Consequently, in order to translate these tuned dynamics to internal DoF, a two-step SEMM is applied; first (38) is solved to obtain $\mathbf{Y}^{\text{tuned}}_{bb}$, which in turn is inserted as an overlay model in (17), (28) or (33).

4. Example: benchmark structure

This section demonstrates the practical applicability of SEMM for the typical use of mixing a 'small' experimental model with the DoF-space of a full numerical model. The example uses the benchmark structure depicted in Figure 10, used previously to validate experimental dynamic substructuring and transfer path analysis methods; see [25, 26]. It is a system consisting of three substructures, denoted A, B and R, that can be coupled in multiple configurations. This example uses substructures A and B only: A is a solid aluminium structure (loosely shaped after the character itself) with a stepper-motor attached; B is a steel structure featuring a honeycomb-like plate with numerous out-of-plane vibration modes.

4.1. Introduction

The envisioned end goal of this study is to couple models of substructures A and B in the two-point coupling configuration using LM-FBS in a frequency range of 0 to 3000 Hz. As can be understood from the figure, coupling of rotational dynamics is essential for this test case in order to realise complete coupling behaviour. Therefore we will first seek to determine high-quality 6-DoF models of the dynamics at each

coupling point, i.e. comprising three translations and three rotations. To that end, the Virtual Point Transformation (VPT) method will be employed to construct virtual nodes with full 6-DoF dynamics, derived from an overdetermined set of translational FRF around each coupling point[6].

In practice, for a 6-DoF virtual node, this means using at least three tri-axial sensors and applying more than six linearly independent impact directions. For a structure consisting of multiple coupling points this might not be easy or feasible, for instance due to the high required sensor count or added weight limitations. The predominant advantage of an expansion method like SEMM is thus that it is theoretically possible to perform an experiment with fewer sensors and expand to DoF which have not been measured. This way, a sufficiently large DoF-basis can be acquired to perform the virtual point transformation, which can then be used to determine the 6-DoF virtual nodes[7] for the coupling points of the substructures.

In this example of SEMM, a modest set of measured DoF on substructure A is used as the overlay model and an associated parent model is constructed from an FE model. The resulting hybrid model follows the dynamics of the measurement, hence represents the dynamics of the actual component. It will thus be shown that an experimental DoF-set, essentially insufficient for virtual point modelling, can be used to construct a high-quality hybrid model for the entire frequency range of 0 to 3000 Hz. Additionally, with the use of the trust function of section 3.3, dynamics of the numerical model are inserted in the low-frequency band to complement the experimental data that is untrustworthy at these low frequencies.

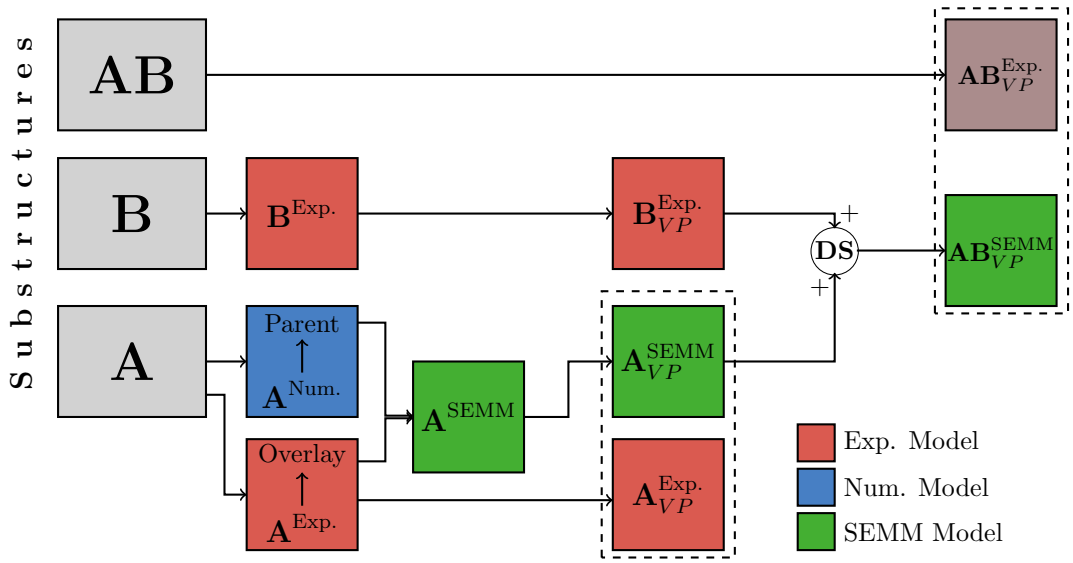

Figure 11: The system at hand consists of substructures A and B. Substructure A is modelled both numerically and experimentally and the parent and overlay models are extracted respectively. SEMM is performed with the parent and overlay model as described by equation (28). A VP transformation is applied on the hybrid model and it is validated by direct comparison with the VP transformed experimental model of A. The hybrid model is subsequently coupled to the VP transformed experimental model of substructure B and this is compared to the experimental measurements of the full-system model AB.

4.2. Application

Figure 11 is a flowchart depicting the process applied in this test-case. Substructure A is modelled both numerically and experimentally and will be the candidate for the application of SEMM. The hybrid model of

[6]The mathematical details of the virtual point transformation method are omitted; the interested reader is referred to [11, 12].

[7]Applying the VPT method is in that regard similar to introducing an RBE3 element to interpolate between multiple 3D nodes, which is standard practice in many FE codes.

A will be compared to its experimental counterpart as part of the validation. Thereafter, the hybrid model will be coupled dynamically to substructure B to form a hybrid model AB which is in turn validated by comparison with both a purely experimental FBS model and measurements performed directly on AB.

4.2.1. Experimental overlay model of A

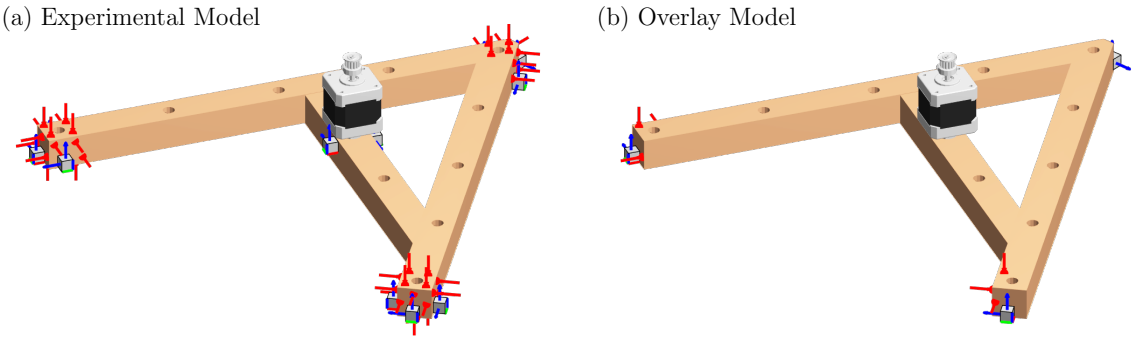

Figure 12: (a): The full experimental measurement sensor (blue) and impact (red) locations. (b): The subset of impact and sensor locations used for the overlay model. Note that the limited number of sensor and impact locations is insufficient for proper virtual point definition.

Impact hammer FRF measurements are performed on structure A to construct an experimental FRF-model. Figure 12a shows the sensor and impact locations used in the experiment, comprising 3 tri-axial accelerometers (i.e. 9 channels) and 16 impact points per coupling point. The measured DoF-set is sufficiently large to construct the virtual points required for coupling, i.e. sufficient independent DoF have been measured near each coupling point.

From this experimental FRF-model, a subset of DoF is used as the overlay model in the SEMM process. This selection of DoF is shown in Figure 12b. Note that with this set the virtual points would be underdetermined, i.e. this DoF-set in itself is not large enough to construct the virtual nodes. The full 'donor' experimental model of A (Figure 12a) is subsequently used to validate the hybrid model of A and used to construct a pure experimental FBS model of AB.

4.2.2. Numerical parent model of A

Additionally, un undamped FE-model is constructed for component A (without the stepper-motor) whose node locations are shown in Figure 13a. This is used to construct a reduced FE-FRF model which will act as the parent. This model contains the overlay DoF-set as well as a set of internal DoF which are used to construct virtual points; these DoF are shown in Figure 13b. Figure 14 is a close up of a virtual point configuration where the red and blue arrows represent the input and output DoF of the model respectively and the green arrows represent the virtual point. Clearly the set of numerically modelled DoF can readily observe and control the virtual point. It should be noted however, that the virtual point transformation itself is not yet performed.

Table 4: The size of the DoF-sets used in the practical case. The overlay model has 9 output DoF and 6 input DoF which are all considered boundary DoF. These are expanded to the 54×54 DoF in the parent model. A full-interface decoupling is used: all internal DoF are kept, and non are discarded (Represented by Figure 7d)

	Internal i	Kept k	Discarded d	Boundary b
Output DoF	54	54	0	9
Input DoF	54	54	0	6

(a) FE-model

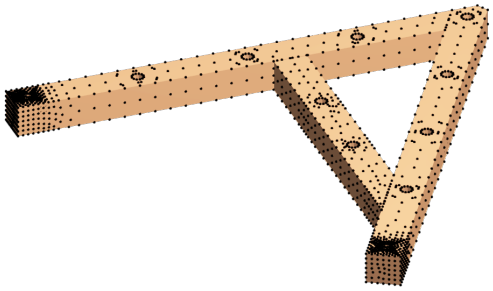

(b) FE-FRF Parent Model

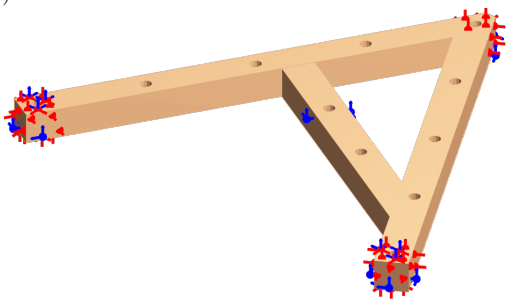

Figure 13: (a): The node locations of the FE model used to construct the numerical FRF model. (b): The DoF locations of the numerical FRF model used as the parent model in the SEMM process. Note that the stepper-motor is not included in the numerical FE-model.

4.2.3. Hybrid model of A

SEMM is applied on the parent and overlay model constructed above by means of a full interface decoupling defined by equation (28). Here all internal DoF are kept in the decoupling step of SEMM (Shown graphically by figure 7d). The resulting SEMM constructed hybrid model follows the experimental dynamics from the overlay model yet can both observe and control the virtual points since it consists of the same DoF-space as the parent model.

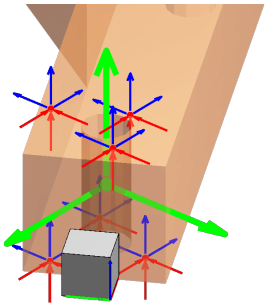

Figure 14: A closer look at the parent model DoF locations of Figure 13b where the sensor location of the overlay model and the virtual point (green) is included. Note that the chosen parent DoF-set is sufficient to properly define this virtual point.

4.2.4. Hybrid and experimental model of AB

The resulting hybrid model is coupled to the experimental model of structure B to form the hybrid model of AB. In order to couple the models the virtual points method is used to construct the collocated virtual nodes at the coupling points; displayed in Figure 14. The coupling itself is done with the LM-FBS method (7) with the virtual point DoF as the boundary DoF.

In order to proper validate the hybrid model of AB a pure experimental DS model is also constructed. This is done by coupling the full set of experimental measurements to the same experimental model of B. Again, this is done with the LM-FBS method on the virtual point nodes.

4.3. Results

The resulting hybrid model is first validated by comparison between the experimental and hybrid FRF, both internally and at the virtual points. Afterwards, the validated hybrid model of A is coupled to the

experimental model of substructure B to form the hybrid model AB. The coupled hybrid AB model is then validated by means of comparison with both the pure experimental coupled model AB and the measurements performed directly on structure AB.

4.3.1. Comparison of the internal DoF

One of the advantages of SEMM is the ability to expand experimental dynamics to DoF other than the ones measured. In Figure 15 the admittance FRF from a force at a virtual point to an acceleration in the centre is shown. Note in Figure 12b that the overlay model has neither sensor, nor impact information available in the centre of structure A, thus the resulting hybrid FRF is based on expansion of experimental (overlay) information in the numerical (parent) structure.

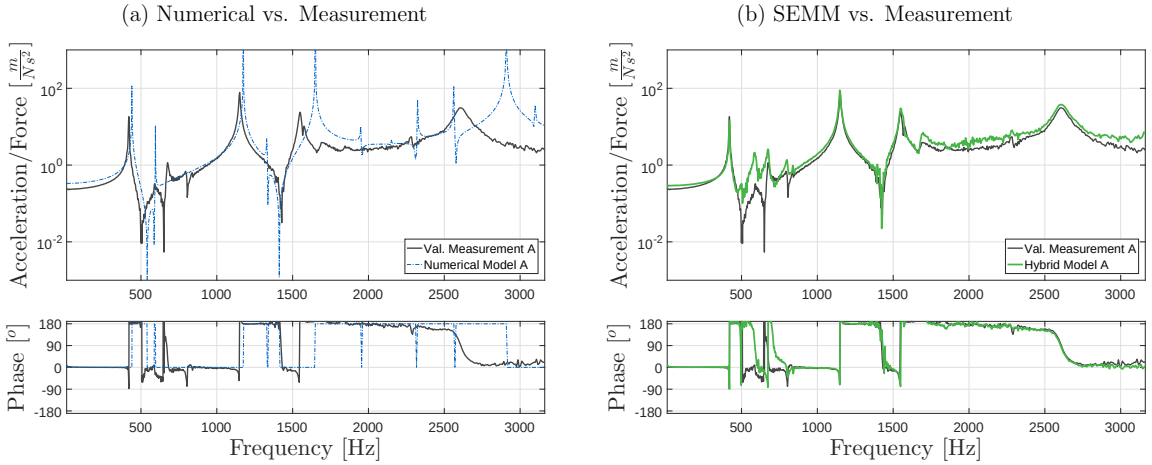

Figure 15: Internal FRF from a corner force to a displacement in x-direction at the centre of the structure. Although the numerical (blue) eigenfrequencies in (a) do not coincide with the experimental eigenfrequencies the hybrid model (green) in (b) follows those of the experimental model. However, the discrepancy between experimental and numerical models causes a stiffness off-set in the hybrid model.

In Figure 15a the reference measurement and the numerically simulated FRF are compared. There are notable discrepancies in the FRF characteristics of interest, i.e. frequency off-set, damping values, and general admittance. This is in great part due to the fact that the motor is not included in the FE-model whilst it is included in the measurements. Nevertheless, this numerical model can be used effectively to construct the hybrid model. Figure 15b shows the FRF of the hybrid model as compared to the reference measurement. A relatively large stiffness difference can be seen between 500 and $800\,\mathrm{Hz}$ and from $1600\,\mathrm{Hz}$ onwards, yet the eigenfrequency and damping information of the experiments (overlay) are captured in the hybrid model, as expected. The stiffness differences can be accounted to the fact that input overlay information is dynamically 'far' from the desired internal DoF. The discrepancy between the overlay and removed model (introduced in (23)) is too large in this particular frequency band.

4.3.2. Comparison of the VP DoF

Evidently SEMM can expand an experimental DoF-set with DoF from a parent DoF-set and form independent FRF. Next, we require that the expanded DoF can be used to form physically relevant hybrid virtual points. Therefore, although the hybrid virtual points are derived from minimal experimental data, they should represent the virtual points of the full experimental model. In Figure 16 both a numerically simulated and hybrid driving-point FRF of a virtual point are compared to the experimental reference.

Figure 16b shows that the virtual point constructed in the hybrid model with an underdetermined set of experimental DoF is still representative of the experimental virtual point. This is despite the fact that the

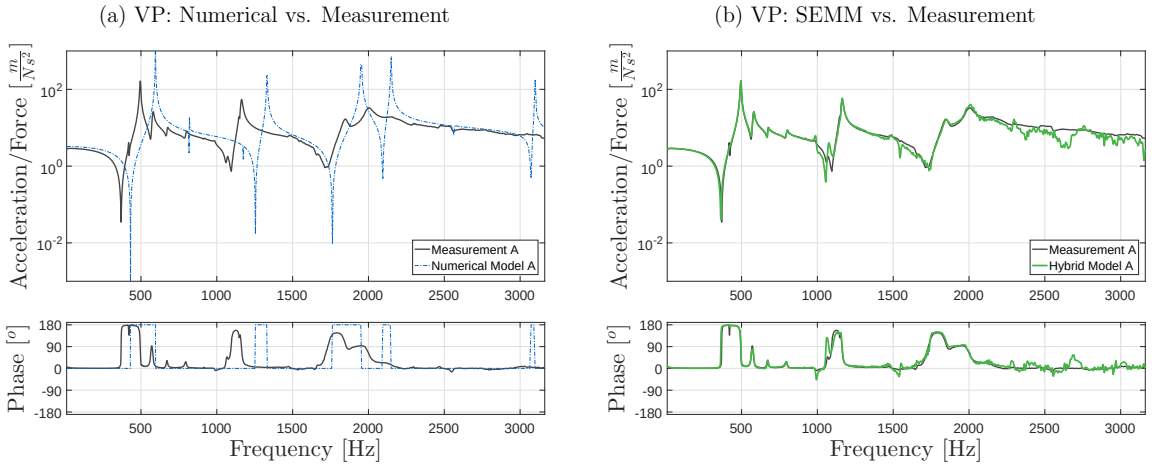

Figure 16: A driving point FRF in the $z-$ direction of virtual point 2. Note that the numerically constructed virtual point (blue) in (a) differs much from the experimental reference, yet the SEMM constructed hybrid model (green) in (b) follows the experimental model up to $3\,\mathrm{kHz}$

numerically simulated virtual point FRF does not properly resemble the measured reference as shown in Figure 16a.

This is possible because SEMM effectively removes the need for mathematical overdetermination of the virtual point; the numerical structure used already ensures mathematical overdetermination. All that is required of the overlay model's DoF-set is that it is representative of the structure's motion in the chosen frequency band which is evident from the FRF results in Figure 15b.

4.3.3. Comparison between coupled and measured AB

The question arises if the virtual point acquired though SEMM is still viable for use in DS. Although Figure's 15 and 16 show that the hybrid model's eigenfrequencies match those of the experimental model; with DS coupling the general stiffness contribution also plays an important role in the coupling since the relation in stiffness of the two models determine the stiffness of the system.

To test the viability of the hybrid virtual points both the hybrid model of AB and the pure experimental coupled model of AB are compared to the measurements on the full-structure AB. The results are shown in Figure 17.

Figure 17 shows driving-point FRF of a virtual point. Both the pure experimental coupled model AB displayed in Figure 17a and the hybrid coupled model AB displayed in Figure 17b closely resemble the reference full-structure measurement in the frequency band up to $1600\,\mathrm{Hz}$. At higher frequencies the FRF for both the pure experimental and the hybrid coupled model diverge from the reference. Since both the SEMM model, and the experimental model are no longer valid, this error is attributed to the DS coupling and not the SEMM method; higher frequencies have thus been left out of the analysis.

A few observations are made however:

- At $440\,\mathrm{Hz}$ there is a eigenfrequency shift of the hybrid coupled model; this is not the case in the pure experimental model. Note that this is in the frequency regime where a flat stiffness difference is observed in the expanded DoF of the hybrid model. It is possibly the cause of a frequency shift in the coupled FRF.
- A large eigenfrequency shift exists between the reference eigenfrequency at $790\,\mathrm{Hz}$ and the hybrid

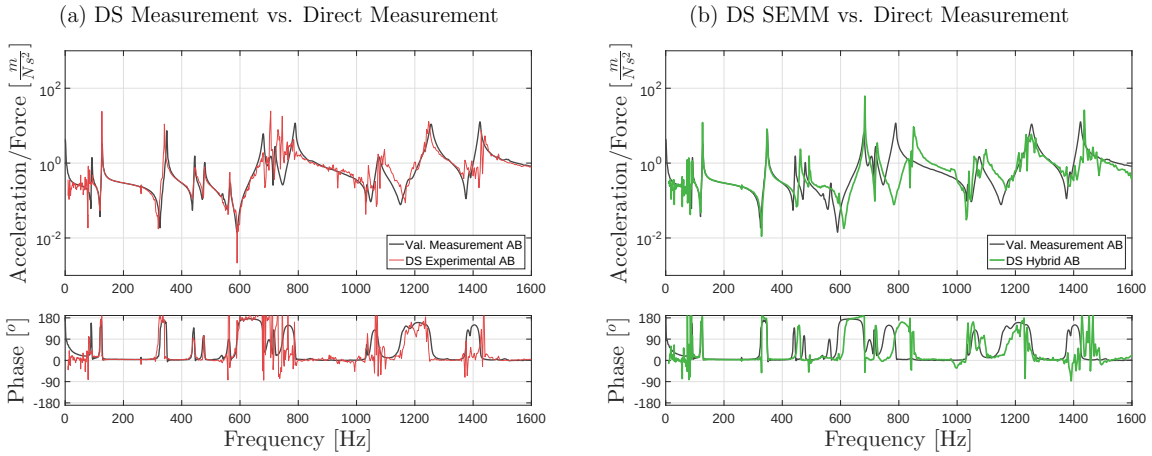

Figure 17: A driving-point FRF in the $z-$ direction of the virtual node 3. Both the pure experimental DS model of AB (a) and the hybrid DS model (b) are compared to a reference measurement of the physical component AB.

eigenfrequency at $840\,\mathrm{Hz}$. It should be noted however, that in the experimental coupled model no eigenfrequency peaks are clearly visible in this frequency range.

- For both the pure experimental and the hybrid coupled model the low-frequency content is poor. This is due to the poor low-frequency measurements of structure A which are passed on to the hybrid model. This is fixed by mixing in trusted numerically simulated FRF with the use of trust functions in the next section.

4.4. Trust function

Depending on the complexity of the structure at hand, experimental models certainly have an advantage over numerical models in the higher frequency domains. At lower frequencies however, experimental models are contaminated by the dynamics of the setup and by the measurement range of the equipment used. This results in low measurement coherence for this particular band. Indeed, in Figure 17 it is clearly seen that the experimental DS results, and consequently the hybrid DS results are very noisy in the lower frequency band. Conversely, numerical models excel in the lower frequency range. They are generally capable of determining the static situation as well as the first modes of a structure.

Using the trust functions introduced in section 3.3 an overlay model can be created which follows trusted numerical dynamics in the lower frequency bands and gradually switches over to experimental dynamics at an appropriate user-defined frequency. Therefore, the hybrid model will circumvent the low coherence measurement of experimental models in the lower frequency but still follow experimental dynamics at the higher frequencies. This results in an hybrid model based on the ”best of both worlds”

For the trust function a switching frequency at $250\,\mathrm{Hz}$ is defined. To ensure that there is no sudden shift in the FRF the model dynamics are gradually shifted over a $100\,\mathrm{Hz}$ frequency band from $100\,\%$ to $0\,\%$ numerical (parent) dynamics. The function is depicted over the resulting FRF in Figure 18b. The trust function is applied to both the hybrid model of structure A, as well as a new hybrid model of structure B. The models are coupled like before to construct an AB hybrid model.

In Figure 18 the resulting hybrid AB model is compared to the measurement of AB as before; focussed on the low frequencies. Due to the use of numerical dynamics in this frequency range, experimental noise is removed from the hybrid model. The trust function ensures a gradual and physically relevant shift to experimental dynamics throughout the given shifting bandwidth.

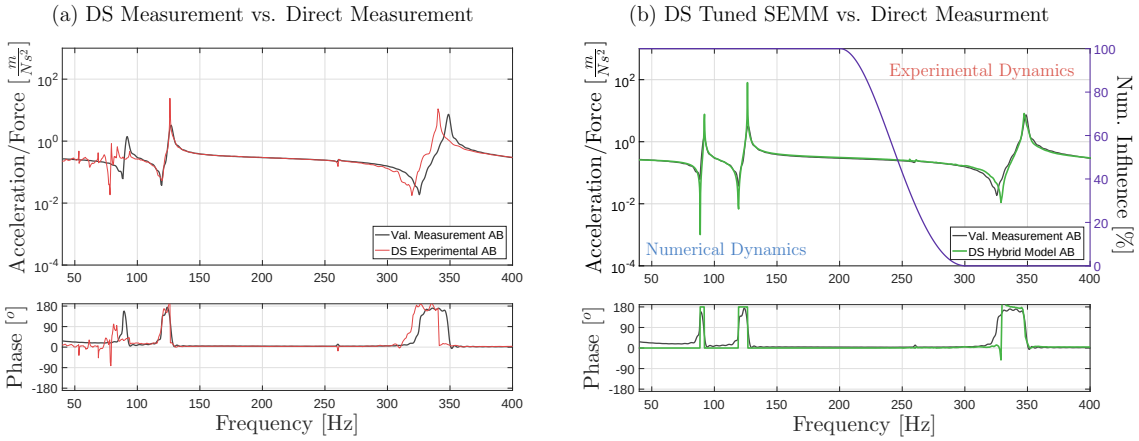

Figure 18: A close-up of the low-frequency band of the driving point FRF in $z-$ direction from Figure 17. Again, the experimental DS (a) and the hybrid DS (b) are compared to the reference measurement. Due to the inclusion of numerical dynamics in the low-frequency band of the hybrid FRF the noise due to low coherence is removed.

5. Discussion

5.1. On the SEMM method

SEMM is explained conceptually as a parent model adapted to follow overlay model dynamics. In effect, the overlay model is expanded to the parent model DoF-set. Therefore the overlay DoF can be regarded as the *master* DoF-set, whereas the parent DoF-set is regarded as the *slave* DoF-set.

Although the overlay model can be regarded as the master model it is still the parent model that provides the basis for the new FRF. The interface conditions ensure that the interface FRF become identical to those of the overlay model yet this is not defined a priori which can result in some practical complications in situations with poor conditioning.

It is stated at the end of section 2.2 that the overlay model is not inverted in the process, while in fact it is inverted twice. This theoretically cancels the inversion, yet in practice this is not the case in situations with poor conditioning. The single-line methods of (21) and (31) avoid this double inversion. Consequently, the single-line method is the preferred method for the application of SEMM. Unfortunately no single-line method is derived for the use of trust-functions.

5.2. On the construction of the input models

The physical interpretation provided in section 2.3 gives an insight into the physical process behind the method. It accentuates the problems inherent in the method, and thereby the demands placed on the parent and overlay model in order to construct adequate hybrid models. The numerical example presented in section 2.4 already illustrates the need for the overlay model to describe the relevant dynamics of the structure, i.e. its representability as a full structure model. In addition, since the method places strict conditions on the full overlay model, it must not be ill-conditioned. In practice, this requires the DoF-set of the (experimental) overlay model to allow sufficient flexibility between DoF. Therefore a balance is needed between the rank-ability and conditioning of the overlay model as a result of the boundary DoF choice[8].

[8]To get an impression of the rank-ability (or observability) and conditioning of the overlay model, one could calculate a singular value breakdown of the overlay FRF matrix and look at the spread of its singular values.

These demands are vastly different than the requirements placed on experimental models destined for e.g. virtual point transformations or multi-point constraints. Indeed, in such cases one needs complete information of each physical connection point from the experiment, leading to large FRF models with relatively poor conditioning. This is in sheer contrast to the focus of overlay models which must predominantly observe not local space, but the full system modal space, as the local space is filled in by the parent model's DoF-set.

No limitations regarding e.g. modal density, proportional damping, or choice of damping model are explicitly made although the influence of these factors to the method's accuracy is still unproven. The hybrid model in the practical case is, for example, created without damping in the parent model, yet other results may be obtained with different damping assumptions. More research into these subjects is warranted.

6. Conclusion

SEMM is presented as a technique that creates a model hybrid by expanding a DoF-set of a certain overlay to a structure of the parent model. This expansion process warrants its comparison with other expansion techniques, such as Guyan expansion, component mode synthesis (CMS) or modal expansion techniques. The main difference between SEMM and the aforementioned techniques is that SEMM allows the existence of 'internal' dynamics otherwise lost in the condensation process. Therefore, even though a DoF-set is expanded, the hybrid model is an integral full-rank model.

The hybrid definition of the model has an inherent problem: the dynamics of parent and overlay model conflict which results in spurious peaks at internal mode frequencies. This is shown in the numerical example of section 2.4. This problem is largely mitigated by the use of extended interface decoupling of section 3.1 where the full model decoupling process completely removes these conflicting modes. Indeed, the full model decoupling has shown the best results in the tests done.

It is shown in the sections that follow that SEMM is a framework rather than a standalone method, allowing for several choices to be made depending on the respective needs of the application. One application that stands out is tested as SEMM is applied practically on a benchmark structure designed for DS validations. It is shown that SEMM allows the expansion of a small experimental DoF-set to a full-rank expanded model by use of an FE model, and that these expanded DoF can be used to construct physically correct virtual points. Furthermore, it is shown that these virtual points can be used to couple models in DS fashion. Finally, it is also demonstrated that numerical dynamic information can be faded in to improve low-frequency dynamics of the resulting hybrid FRF.

The SEMM framework as presented can be regarded as an invaluable extension to the experimentalist's toolkit, with the potential to save measurement time and increase the quality of hybrid dynamic models.

Acknowledgements

This research was made possible by ASML, whose support is deeply acknowledged.

Appendix A. Deriving the single-line method by primal decomposition

In this appendix the single-line method of SEMM is derived for the general single parent model method. This is done with the primal-decomposed admittance notation [27]. The primal-decomposed notation is first derived for SEMM.

The parent, and overlay models are repeated below:

$$\mathbf{Y}^{\text{par}} \triangleq \begin{bmatrix} \mathbf{Y}_{dd} & \mathbf{Y}_{dk} & \mathbf{Y}_{db} \\ \mathbf{Y}_{kd} & \mathbf{Y}_{kk} & \mathbf{Y}_{kb} \\ \mathbf{Y}_{bd} & \mathbf{Y}_{bk} & \mathbf{Y}_{bb} \end{bmatrix}^{\text{par}} \qquad \mathbf{Y}^{\text{ov}} \triangleq \begin{bmatrix} \mathbf{Y}_{bb} \end{bmatrix}^{\text{ov}} \tag{A.1}$$

Note that the differentiation between compatibility and equilibrium kept k and discarded d DoF is omitted here for clarity; this differentiation still applies however. Recall from equation (26) that the removed model is a sub-set of the parent model defined as:

$$\mathbf{Y}^{\text{rem}} \triangleq \begin{bmatrix} \mathbf{Y}_{kk} & \mathbf{Y}_{kb} \\ \mathbf{Y}_{bk} & \mathbf{Y}_{bb} \end{bmatrix}^{\text{par}} \tag{A.2}$$

The derivation is done in two separate steps. First the overlay model is decoupled from the removed model creating a delta model $\mathbf{Y}^{\Delta}$. This delta model is then decoupled from the parent model. This two-step approach is an easier derivation, thus keeping oversight in the process. Let us now define a delta model which is the difference between the overlay and removed model:

$$\mathbf{Y}^{\Delta} \triangleq \mathbf{Y}^{\text{rem}} \; (-) \; \mathbf{Y}^{\text{ov}} \tag{A.3}$$

This model is constructed via the primal-decomposed admittance notation. The equations of motion of the coupled system $\mathbf{Y}^{\Delta}$ are denoted below:

$$\mathbf{Y}^{\text{rem}}(\mathbf{f} + \mathbf{g}^{\text{rem}}) = \mathbf{u}^{\text{rem}} \tag{A.4}$$

$$-\mathbf{Y}^{\text{ov}}\mathbf{g}^{\text{ov}} = \mathbf{u}^{\text{ov}} \tag{A.5}$$

$$\begin{bmatrix} \mathbf{Y}^{\text{rem}}_{kk} & \mathbf{Y}^{\text{rem}}_{kb} & \mathbf{0} \\ \mathbf{Y}^{\text{rem}}_{bk} & \mathbf{Y}^{\text{rem}}_{bb} & \mathbf{0} \\ \mathbf{0} & \mathbf{0} & -\mathbf{Y}^{\text{ov}}_{bb} \end{bmatrix} \left(\begin{bmatrix} \mathbf{f}_k \\ \mathbf{f}_b \\ \mathbf{0} \end{bmatrix} + \begin{bmatrix} \mathbf{0} \\ \mathbf{g}^{\text{rem}}_b \\ \mathbf{g}^{\text{ov}}_b \end{bmatrix} \right) = \begin{bmatrix} \mathbf{u}^{\text{rem}}_k \\ \mathbf{u}^{\text{rem}}_b \\ \mathbf{u}^{\text{ov}}_b \end{bmatrix} \tag{A.6}$$

s.t.

$$\mathbf{g}^{\text{rem}}_b + \mathbf{g}^{\text{ov}}_b = \mathbf{0} \tag{A.7}$$

$$\mathbf{u}^{\text{rem}}_b - \mathbf{u}^{\text{ov}}_b = \mathbf{0} \tag{A.8}$$

A Lagrange multiplier $\boldsymbol{\lambda}$ is introduced:

$$\boldsymbol{\lambda} = \mathbf{g}^{\text{rem}}_b = -\mathbf{g}^{\text{ov}}_b \tag{A.9}$$

$\boldsymbol{\lambda}$ is substituted into (A.6) to form:

$$\begin{bmatrix} \mathbf{Y}^{\text{rem}}_{kk} & \mathbf{Y}^{\text{rem}}_{kb} \\ \mathbf{Y}^{\text{rem}}_{bk} & \mathbf{Y}^{\text{rem}}_{bb} \\ \mathbf{0} & \mathbf{Y}^{\text{ov}}_{bb} \end{bmatrix} \begin{bmatrix} \mathbf{f}_k \\ \boldsymbol{\lambda} \end{bmatrix} = \begin{bmatrix} \mathbf{u}^{\text{rem}}_k - \mathbf{Y}^{\text{rem}}_{kb}\mathbf{f}_b \\ \mathbf{u}^{\text{rem}}_b - \mathbf{Y}^{\text{rem}}_{bb}\mathbf{f}_b \\ \mathbf{u}^{\text{ov}}_b \end{bmatrix} \tag{A.10}$$

s.t.

$$\mathbf{u}^{\text{rem}}_b - \mathbf{u}^{\text{ov}}_b = \mathbf{0} \tag{A.11}$$

Finally, by subtracting the third row from the second row in (A.10) the primal decomposed admittance notation becomes:

$$\begin{bmatrix} \mathbf{Y}^{\text{rem}}_{kk} & \mathbf{Y}^{\text{rem}}_{kb} \\ \mathbf{Y}^{\text{rem}}_{bk} & \mathbf{Y}^{\text{rem}}_{bb} - \mathbf{Y}^{\text{ov}}_{bb} \end{bmatrix} \begin{bmatrix} \mathbf{f}_k \\ \boldsymbol{\lambda} \end{bmatrix} = \begin{bmatrix} \mathbf{u}^{\text{rem}}_k - \mathbf{Y}^{\text{rem}}_{kb}\mathbf{f}_b \\ -\mathbf{Y}^{\text{rem}}_{bb}\mathbf{f}_b \end{bmatrix} \tag{A.12}$$

Which is solved for $\boldsymbol{\lambda}$ and $\mathbf{u}$:

$$\boldsymbol{\lambda} = -\left(\mathbf{Y}_{bb}^{\text{rem}} - \mathbf{Y}_{bb}^{\text{ov}}\right)^{-1} \begin{bmatrix}\mathbf{Y}_{bk} & \mathbf{Y}_{bb}\end{bmatrix}^{\text{rem}} \mathbf{f} \tag{A.13}$$

$$\mathbf{u} = \mathbf{Y}^{\text{rem}}\mathbf{f} + \begin{bmatrix}\mathbf{Y}_{kb} \\ \mathbf{Y}_{bb}\end{bmatrix}^{\text{rem}} \boldsymbol{\lambda} \tag{A.14}$$

Substituting (A.13) into (A.14):

$$\mathbf{u} = \mathbf{Y}^{\text{rem}}\mathbf{f} - \begin{bmatrix}\mathbf{Y}_{kb} \\ \mathbf{Y}_{bb}\end{bmatrix}^{\text{rem}} \left(\mathbf{Y}_{bb}^{\text{rem}} - \mathbf{Y}_{bb}^{\text{ov}}\right)^{-1} \begin{bmatrix}\mathbf{Y}_{bk} & \mathbf{Y}_{bb}\end{bmatrix}^{\text{rem}} \mathbf{f} \tag{A.15}$$

From equation (A.15) the delta model $\mathbf{Y}^{\Delta}$ is formulated. Note that this is the primal notation analogue to the dual-decomposed LM-FBS method of equation (5), as expected. The delta model $\mathbf{Y}^{\Delta}$ becomes:

$$\mathbf{Y}^{\Delta} = \begin{bmatrix}\mathbf{Y}^{\text{rem}}\end{bmatrix} - \begin{bmatrix}\mathbf{Y}_{kb} \\ \mathbf{Y}_{bb}\end{bmatrix}^{\text{rem}} \left(\mathbf{Y}_{bb}^{\text{rem}} - \mathbf{Y}_{bb}^{\text{ov}}\right)^{-1} \begin{bmatrix}\mathbf{Y}_{bk} & \mathbf{Y}_{bb}\end{bmatrix}^{\text{rem}} \tag{A.16}$$

This delta model is removed from the parent model thus effectively removing the removed model and adding the overlay model. The hybrid model $\mathbf{Y}^{\text{SEMM}}$ is defined as:

$$\begin{aligned}\mathbf{Y}^{\text{SEMM}} &\triangleq \mathbf{Y}^{\text{par}} \,(-)\, \mathbf{Y}^{\text{rem}} \,(+)\, \mathbf{Y}^{\text{ov}} && \text{(A.17)}\\ &= \mathbf{Y}^{\text{par}} \,(-)\, \left(\mathbf{Y}^{\text{rem}} \,(-)\, \mathbf{Y}^{\text{ov}}\right) \\ &= \mathbf{Y}^{\text{par}} \,(-)\, \mathbf{Y}^{\Delta} && \text{(A.18)}\end{aligned}$$

Following the same derivation as above it can be shown that the hybrid model $\mathbf{Y}^{\text{SEMM}}$ becomes:

$$\begin{aligned}\mathbf{Y}^{\text{SEMM}} &= \begin{bmatrix}\mathbf{Y}\end{bmatrix}^{\text{par}} - \begin{bmatrix}\mathbf{Y}_{ik} & \mathbf{Y}_{ib} \\ \mathbf{Y}_{bk} & \mathbf{Y}_{bb}\end{bmatrix}^{\text{par}} \left(\begin{bmatrix}\mathbf{Y}_{kk} & \mathbf{Y}_{kb} \\ \mathbf{Y}_{bk} & \mathbf{Y}_{bb}\end{bmatrix}^{\text{par}} - \mathbf{Y}^{\Delta}\right)^{-1} \begin{bmatrix}\mathbf{Y}_{ki} & \mathbf{Y}_{kb} \\ \mathbf{Y}_{bi} & \mathbf{Y}_{bb}\end{bmatrix}^{\text{par}} && \text{(A.19)}\\ &= \begin{bmatrix}\mathbf{Y}\end{bmatrix}^{\text{par}} - \begin{bmatrix}\mathbf{Y}_{ik} & \mathbf{Y}_{ib} \\ \mathbf{Y}_{bk} & \mathbf{Y}_{bb}\end{bmatrix}^{\text{par}} \mathbf{Z}_{\text{int}} \begin{bmatrix}\mathbf{Y}_{ki} & \mathbf{Y}_{kb} \\ \mathbf{Y}_{bi} & \mathbf{Y}_{bb}\end{bmatrix}^{\text{par}} && \text{(A.20)}\end{aligned}$$

Where the coupling interface stiffness $\mathbf{Z}_{\text{int}}$ is:

$$\begin{aligned}\mathbf{Z}_{\text{int}} &= \left(\begin{bmatrix}\mathbf{Y}_{kk} & \mathbf{Y}_{kb} \\ \mathbf{Y}_{bk} & \mathbf{Y}_{bb}\end{bmatrix}^{\text{par}} - \mathbf{Y}^{\Delta}\right)^{-1} && \text{(A.21)}\\ &= \left(\begin{bmatrix}\mathbf{Y}_{kk} & \mathbf{Y}_{kb} \\ \mathbf{Y}_{bk} & \mathbf{Y}_{bb}\end{bmatrix}^{\text{par}} - \begin{bmatrix}\mathbf{Y}^{\text{rem}}\end{bmatrix} + \begin{bmatrix}\mathbf{Y}_{kb} \\ \mathbf{Y}_{bb}\end{bmatrix}^{\text{rem}} \left(\mathbf{Y}_{bb}^{\text{rem}} - \mathbf{Y}_{bb}^{\text{ov}}\right)^{-1} \begin{bmatrix}\mathbf{Y}_{bk} & \mathbf{Y}_{bb}\end{bmatrix}^{\text{rem}}\right)^{-1} && \text{(A.22)}\\ &= \left(\begin{bmatrix}\mathbf{Y}_{kb} \\ \mathbf{Y}_{bb}\end{bmatrix}^{\text{rem}} \left(\mathbf{Y}_{bb} - \mathbf{Y}_{bb}^{\text{ov}}\right)^{-1} \begin{bmatrix}\mathbf{Y}_{bk} & \mathbf{Y}_{bb}\end{bmatrix}^{\text{rem}}\right)^{-1} && \text{(A.23)}\\ &= \left(\begin{bmatrix}\mathbf{Y}_{bk} & \mathbf{Y}_{bb}\end{bmatrix}^{\text{rem}}\right)^{+} \left(\mathbf{Y}_{bb}^{\text{rem}} - \mathbf{Y}^{\text{ov}}\right) \left(\begin{bmatrix}\mathbf{Y}_{kb} \\ \mathbf{Y}_{bb}\end{bmatrix}^{\text{rem}}\right)^{+} && \text{(A.24)}\end{aligned}$$

Note the use of (A.2) to cancel the first two terms of (A.22) to form (A.23). Also note in (A.23) that the formulation that is required to be inverted is singular as the rank is determined by the size of the boundary which is generally smaller than the full size. Hence (A.24) is a generalized inverse.

(A.24) is inserted in (A.20) to form the single-line method of (31) which is repeated here:

$$\mathbf{Y}^{\text{SEMM}} = \begin{bmatrix}\mathbf{Y}\end{bmatrix}^{\text{par}} - \begin{bmatrix}\mathbf{Y}_{ik} & \mathbf{Y}_{ib} \\ \mathbf{Y}_{bk} & \mathbf{Y}_{bb}\end{bmatrix}^{\text{par}} \left(\begin{bmatrix}\mathbf{Y}_{bk} & \mathbf{Y}_{bb}\end{bmatrix}^{\text{rem}}\right)^{+} \left(\mathbf{Y}_{bb}^{\text{rem}} - \mathbf{Y}^{\text{ov}}\right) \left(\begin{bmatrix}\mathbf{Y}_{kb} \\ \mathbf{Y}_{bb}\end{bmatrix}^{\text{rem}}\right)^{+} \begin{bmatrix}\mathbf{Y}_{ki} & \mathbf{Y}_{kb} \\ \mathbf{Y}_{bi} & \mathbf{Y}_{bb}\end{bmatrix}^{\text{par}} \tag{A.25}$$

It is observed that the formulation (A.25) can be implemented directly; this circumvents any numerical problems cause by double inversions.

References

[1] B. Jetmundsen, R. Bielawa, W. G. Flannelly, "Generalized frequency domain substructure synthesis", *Journal of the American Helicopter Society*, 33(1):55–64, 1988, DOI: 10.4050/JAHS.33.55.

[2] D. de Klerk, D. J. Rixen, S. N. Voormeeren, "General framework for dynamic substructuring: History, review and classifcation of techniques", *AIAA Journal*, 46(8):1169–1181, 2008, DOI: 10.2514/1.33274.

[3] P. Sjövall, T. Abrahamsson, "Component system identification and state-space model synthesis", *Mechanical Systems & Signal Processing*, 21(7):2697–2714, 2007, DOI: 10.1016/j.ymssp.2007.03.002.

[4] M. Allen, R. Mayes, "Comparison of FRF and modal methods for combining experimental and analytical substructures", in: *Proceedings of the XXV International Modal Analysis Conference (IMAC), Orlando, FL*, Society for Experimental Mechanics, Bethel, CT, 2007.

[5] E. Balmès, "Integration of existing methods and user knowledge in a mimo identification algorithm for structures with high modal densities", in: *11th International Modal Analysis Conference - Modal Testing and Analysis - for Solutions that Fit*, Proceedings of the 11th IMAC, A Conference and Exposition on Structural Dynamics, 613–619, 1993.

[6] E. Balmès, "Frequency domain identification of structural dynamics using the pole/residue parametrization", in: *IMAC XIV - 14th International Modal Analysis Conference - Noise and Vibration Harshness (NVH)*, Proceedings of the 14th IMAC, A Conference and Exposition on Structural Dynamics, 1996.

[7] R. R. J. Craig, M. C. C. Bampton, "Coupling of substructures using component mode synthesis", *AIAA Journal*, 6(7):1313–1319, 1968, DOI: 10.2514/3.2947.

[8] J. C. O'Callahan, P. Avitabile, R. Riemer, "System equivalent reduction expansion process (SEREP)", in: *Proceedings of the VII International Modal Analysis Conference (IMAC), Boston, MA*, volume 1, 29–37, Society for Experimental Mechanics, Bethel, CT, 1989.

[9] L. Thibault, A. Butland, P. Avitabile, "Variability improvement of key inaccurate node groups–viking", in: *Topics in Modal Analysis II, Volume 6*, Conference Proceedings of the Society for Experimental Mechanics Series, 603–624, Springer New York, 2012, DOI: 10.1007/978-1-4614-2419-2˙61.

[10] D. de Klerk, D. Rixen, S. Voormeeren, F. Pasteuning, "Solving the RDoF problem in experimental dynamic substructuring", in: *Proceedings of the XXVI International Modal Analysis Conference (IMAC), Orlando, FL*, Society for Experimental Mechanics, Bethel, CT, 2008.

[11] M. V. van der Seijs, D. D. van den Bosch, D. J. Rixen, D. de Klerk, "An improved methodology for the virtual point transformation of measured frequency response functions in dynamic substructuring", in: M. Papadrakakis, V. Papadopoulos, V. Plevris (eds.), *4th ECCOMAS Thematic Conference on Computational Methods in Structural Dynamics and Earthquake Engineering (COMPDYN)*, 4334–4347, Kos Island, Greece, 2013.

[12] M. V. van der Seijs, *Experimental dynamic substructuring: Analysis and design strategies for vehicle development*, Ph.D. thesis, Delft University of Technology, 2016, DOI: 10.4233/uuid:28b31294-8d53-49eb-b108-284b63edf670.

[13] M. Allen, R. Mayes, E. Bergman, "Experimental modal substructuring to couple and uncouple substructures with flexible fixtures and multi-point connections", *Journal of Sound & Vibration*, 329(23):4891–4906, 2010, DOI: 10.1016/j.jsv.2010.06.007.

[14] S. Voormeeren, D. Rixen, "A family of substructure decoupling techniques based on a dual assembly approach", *Mechanical Systems & Signal Processing*, 27(18):379, 2012, DOI: 10.1016/j.ymssp.2011.07.028.

[15] W. D'Ambrogio, A. Fregolent, "Replacement of unobservable coupling dofs in substructure decoupling", *Mechanical Systems & Signal Processing*, 95:380–396, 2017, DOI: 10.1016/j.ymssp.2017.03.038.

[16] M. V. van der Seijs, D. de Klerk, D. J. Rixen, S. Rahimi, "Validation of current state frequency based substructuring technology for the characterisation of steering gear – vehicle interaction", in: *Topics in Experimental Dynamic Substructuring, Volume 2*, Proceedings of the 31st IMAC, A Conference on Structural Dynamics, chapter 20, 253–266, Springer New York, 2013, DOI: 10.1007/978-1-4614-6540-9˙20.

[17] D. de Klerk, D. Rixen, J. de Jong, "The frequency based substructuring method reformulated according to the dual domain decomposition method", in: *Proceedings of the XXIV International Modal Analysis Conference (IMAC), St. Louis, MO*, Society for Experimental Mechanics, Bethel, CT, 2006.

[18] D. Rixen, "How measurement inaccuracies induce spurious peaks in frequency based substructuring", in: *Proceedings of the XXVI International Modal Analysis Conference (IMAC), Orlando, FL*, Society for Experimental Mechanics, Bethel, CT, 2008.

[19] W. C. Hurty, "Vibrations of structural systems by Component Mode Synthesis", *Journal of the Engineering Mechanics Division*, 86(4):51–70, 1960.

[20] P. Avitabile, "Model reduction and model expansion and their applications part 1 – theory", in: *Proceedings of the XXIII International Modal Analysis Conference (IMAC), Orlando, FL*, Society for Experimental Mechanics, Bethel, CT, 2005.

[21] S. N. Voormeeren, *Dynamic Substructuring Methodologies for Integrated Dynamic Analysis of Wind Turbines*, Ph.D. thesis, Delft University of Technology, The Netherlands, 2012, DOI: 10.4233/uuid:f45f0548-d5ec-46aa-be7e-7f1c2b57590d.

[22] W. D'Ambrogio, A. Fregolent, "Inverse dynamic substructuring using the direct hybrid assembly in the frequency domain", *Mechanical Systems & Signal Processing*, 45(2):360–377, 2014, DOI: 10.1016/j.ymssp.2013.11.007.

[23] P. Reuss, B. Zeumer, J. Herrmann, L. Gaul, "Consideration of interface damping in dynamic substructuring", in: *Topics in Experimental Dynamics Substructuring and Wind Turbine Dynamics, Volume 2*, Proceedings of the 30th IMAC, A Conference on Structural Dynamics, chapter 10, 81–88, Springer New York, 2012, DOI: 10.1007/978-1-4614-2422-2˙10.

[24] E. Barten, M. V. van der Seijs, D. de Klerk, "A complex power approach to characterise joints in experimental dynamic substructuring", in: *Dynamics of Coupled Structures, Volume 1*, Proceedings of the 32nd IMAC, A Conference and Exposition on Structural Dynamics, chapter 27, 281–296, Springer New York, 2014, DOI: 10.1007/978-3-319-04501-6˙27.

[25] M. V. van der Seijs, E. A. Pasma, D. D. van den Bosch, M. W. F. Wernsen, "A benchmark structure for validation of experimental substructuring, transfer path analysis and source characterisation techniques", in: *Dynamics of Coupled Structures, Volume 4*, Conference Proceedings of the Society for Experimental Mechanics Series, chapter 26, 295–305, Springer New York, 2017, DOI: 10.1007/978-3-319-54930-9˙26.

[26] M. Wernsen, M. van der Seijs, D. de Klerk, "An indicator sensor criterion for in-situ characterisation of source vibrations", in: *Sensors and Instrumentation, Volume 5*, Conference Proceedings of the Society for Experimental Mechanics Series, chapter 7, 55–69, Springer New York, 2017, DOI: 10.1007/978-3-319-54987-3˙7.

[27] D. J. Rixen, A. Boogaard, M. V. van der Seijs, G. van Schothorst, T. van der Poel, "Vibration source description in substructuring: A theoretical depiction", *Mechanical Systems & Signal Processing*, 60–61:498–511, 2015, DOI: 10.1016/j.ymssp.2015.01.024.